Late Pleistocene glaciations on the sub-Antarctic Kerguelen Archipelago: new evidence from 36Cl CRE dating and comparison with other southern mid-latitude glacier records

Joanna Charton, Irene Schimmelpfennig, Vincent Jomelli, Deborah Verfaillie, Guillaume Delpech, Damien Guillaume, Vincent Favier, Laurie Menviel, Thierry Robert, Vincent Rinterknecht, et al.

Late Pleistocene glaciations on the sub-Antarctic Kerguelen Archipelago: new evidence from ^{36}Cl CRE dating and comparison with other southern mid-latitude glacier records

Joanna Charton[a], Irene Schimmelpfennig[a], Vincent Jomelli[a], Deborah Verfaillie[a], Guillaume Delpech[b], Damien Guillaume[c], Vincent Favier[d], Laurie Menviel[e], Thierry Robert[f], Vincent Rinterknecht[a], Claude Legentil[g], ASTER Team[a,1]

[a]*Aix Marseille Univ, CNRS, IRD, INRAE, CEREGE, Aix-en-Provence, France*
[b]*Université Paris-Saclay, CNRS, GEOPS - France*
[c]*Université Jean Monnet Saint-Etienne, CNRS, LGL-TPE UMR5276, F-42023, Saint-Etienne, France*
[d]*Institut des Géosciences de l'Environnement, Université Grenoble Alpes, CNRS, Grenoble, France*
[e]*Climate Change Research Centre, The Australian Centre for Excellence in Antarctic Science, University of New South Wales, Sydney, NSW 2052, Australia*
[f]*Université Paris-Saclay, CNRS, AgroParisTech, Ecologie Systématique Evolution, 91405, Orsay, France*
[g]*Université Paris 1 Panthéon-Sorbonne, CNRS Laboratoire de Géographie Physique - France*

[1]*ASTER Team: Georges Aumaître, Didier Bourlès, Karim Keddadouche*

*Corresponding author: Joanna Charton, charton@cerege.fr

Abstract:

Previous paleo-glacial studies on Kerguelen showed a singular pattern of Holocene glacier evolution on this archipelago in comparison with other southern mid-latitude glacier records. In this study, we aim to test this singularity on a longer timescale, based on 26 new *in situ*-produced ^{36}Cl ages from pre-Holocene glacio-geomorphic features. Samples from moraine boulders and glacially polished bedrock were extracted at six different sites, located near the Port-aux-Français scientific station (PAF site), on Longue Island, Australia Island, on the Port-Jeanne d'Arc Peninsula (PJDA site), on the Gallieni Peninsula at Baie Larose (BLR site) and the McMurdo Island. The moraine ages indicate that glacier culminations occurred during Marine Isotopic Stage 3 (MIS 3) at 42.2 ± 4.9 ka on the PAF site, and during the global Last Glacial Maximum (gLGM) at 21.5 ± 3.2 ka on the PJDA site and at 21.4 ± 3.7 ka and 19.4 ±

2.6 on Baie Larose site. This is the first time that Late Pleistocene glacier culminations are evidenced on Kerguelen by direct moraine dating, thus allowing comparison with other moraine records from the southern mid-latitudes. While it remains speculative whether or not the MIS 3 glacial maximum at ~42.2 ka is in phase with other glaciers at this latitude (due to high age uncertainties), the gLGM glacial maximum is synchronous with that in other southern mid-latitude regions. ^{36}Cl CRE ages of glacially polished bedrock surfaces sampled in different locations of the archipelago vary from ~39 ka to ~19 ka. We interpret these results as reflecting periods of deglaciation that occurred in between the two glacier culminations and right after the gLGM on Kerguelen. These ages also suggest that some places of the archipelago were free of ice at least since ~ 39 ka. The presence of a MIS 3 moraine at PAF site that has not been obliterated by a gLGM advance suggests that the ~ 42.2 ka glacier extent was at least as large as gLGM glacial maxima on the archipelago. The glacier culmination during MIS 3 being larger than that during the gLGM on the Kerguelen Archipelago matches observations in other southern mid-latitude regions. Late Pleistocene glacier culminations on Kerguelen may have been in phase with cold temperatures recorded in SST records, which suggest a cooling around Kerguelen. However, climate drivers responsible for the larger MIS 3 glacier culmination on Kerguelen still remain unclear even if we hypothesize that changes in precipitation may have superimposed on temperature changes.

Keywords: glacier fluctuations; paleoclimate; ^{36}Cl CRE dating; Late Pleistocene; Marine Isotopic Stage 3; Marine Isotopic Stage 2; Last Glacial Maximum; Southern mid-latitudes; sub-Antarctic; Kerguelen Islands.

1. Introduction

Southern Hemisphere terrestrial glacier evolutions since the beginning of Marine Isotopic Stage 3 (MIS 3; 60 - 26.5 ka) remain less constrained than in the Northern Hemisphere. In addition, most of the existing long-term paleoglacier data are documented in New Zealand (*e.g.*, Denton et al., 2021) and Patagonia (*e.g.*, Garcia et al., 2018) and remain scarce in other parts of the sub-Antarctic sector (*e.g.*, Rudolph et al., 2020), due to the predominance of small islands with underwater moraines and limited terrestrial records of glacier fluctuations (Fig. 1). Yet, the sub-Antarctic islands constitute key targets relevant to the reconstruction of local glacier evolution and regional climate mechanisms with regard to the effects of the latitudinal migration of the Southern Westerly Winds and hydrological fronts (*e.g.*, the Antarctic Polar Front). Recent investigations on Holocene glacier fluctuations in the southern mid-latitudes, based on cosmic-ray exposure (CRE) dating of glacio-geomorphological landforms showed that glacier behavior differs depending on the region during the Holocene (Charton et al., 2022). One of the regions where the glacier pattern during the Holocene was particularly divergent is the sub-Antarctic Kerguelen Archipelago (49°S, 69°E), located in the southern Indian Ocean. Existing chronological constraints from erratic boulders and bedrock surface ages only provided a general idea of the glacier extents and retreat dynamics prior to the Late Glacial period on Kerguelen (Jomelli et al., 2018). However, direct moraine dating from MIS 3 and the gLGM are lacking so far, preventing a meaningful comparison with the records in other regions (*e.g.*, New Zealand, Patagonia). Glacier reconstructions from other regions of the southern mid-latitudes indicate major glacier extents during MIS 3 (*e.g.*, in New Zealand, Strand et al., 2019), which are often characterized in the literature as an early local Last Glacial Maximum (*e.g.*, Rudolph et al., 2020), as they constitute a larger glacier advance than during the global Last Glacial Maximum (gLGM; 26.5 - 19 ka; Clark et al., 2009). Moreover, glaciers

from the southern mid-latitudes also frequently experienced advances and/or stagnations during the gLGM (*e.g.*, Leger et al., 2021; Tielidze et al., 2022), synchronously with ice sheets reaching their maxima at the time of the globally lowest sea level (Clark et al., 2009).

Here we use direct moraine dating to tackle the question whether glaciers located on the Kerguelen Archipelago *(i)* experienced an early local Last Glacial Maximum during the MIS 3 period consistent with other regions from the southern mid-latitudes and *(ii)* re-advanced during the gLGM in line with the global-scale maximum extent of mountain glaciers and ice sheets. Answering these questions will also allow us to understand if the archipelago was totally covered by ice during either MIS 3 or the gLGM and explore possible climatic mechanisms.

To that end, we provide 26 new ^{36}Cl CRE ages from moraine boulders and glacially polished bedrock samples. This dataset includes samples from six different sites of the Kerguelen Archipelago, which improves our understanding of Late Pleistocene glaciation at the archipelago's scale and therefore the climatic conditions responsible for such glacial activity.

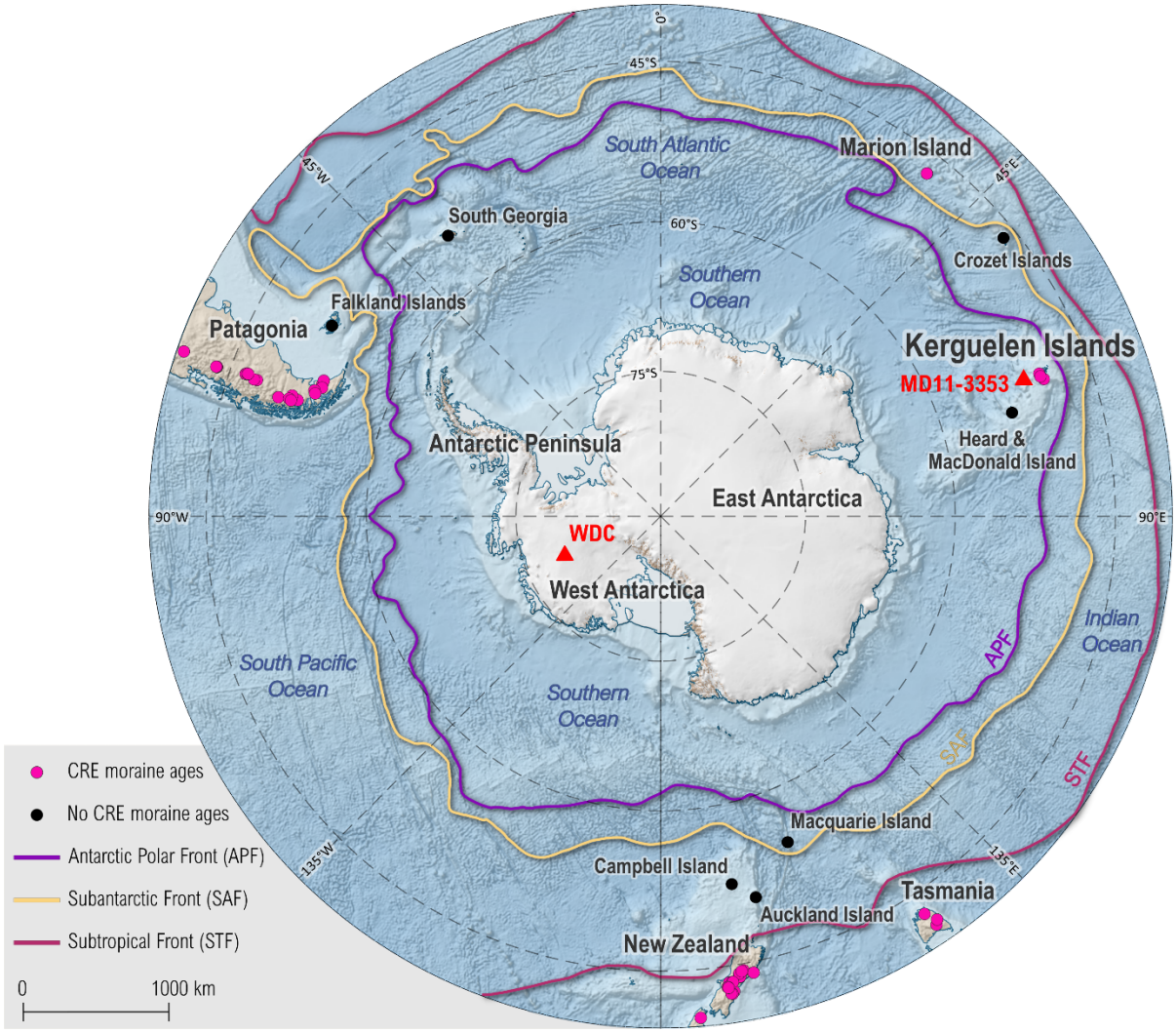

Fig. 1 - Regional setting of the Kerguelen Archipelago in relation to other mid-latitude regions of the Southern Hemisphere and the Southern Ocean, with schematic physical oceanography from Mazloff et al. (2010). Sites referred to in the text are annotated, in particular the climatic proxies (red triangles) discussed in section 5.3. Please note that legend refers to CRE moraine ages during the investigated period, i.e., from ~45 ka to ~19 ka. Background map is from the geospatial data package Quantarctica (Matsuoka et al., 2021 and references therein).

2. Regional setting

The sub-Antarctic Kerguelen archipelago is located in the southern Indian Ocean at a latitude of 49°S and longitude of 69°E (Fig. 1). Both the volcanic and glacial activities have shaped the topography of the archipelago, whose highest peak Mt Ross culminates at 1850 m asl. Indeed, the landscape of the archipelago is mostly characterized by a basaltic/volcanic substratum, that is almost entirely dissected by large former glacial valleys and fjords and rare vegetation (Fig. 2). Kerguelen Archipelago's surface area (7215 km^2) is the emerged part of the large Kerguelen-Heard oceanic plateau formed by the Kerguelen plume (Giret et al., 2003). The archipelago is mainly composed of piles of basaltic lavas (flood basalts) emplaced between 30 and 24 Ma but younger volcanism occurs in the southeast provinces and during the Quaternary on the Rallier du Baty Peninsula and at Mont Ross in the Gallieni province (<1 Ma) (Fig. 2). Locally some (large) plutonic bodies were emplaced at depth in the crust; the large syenite laccolith in the Rallier du Baty Peninsula being the best example (Ponthus, 2018). At present, Kerguelen is located south of the Antarctic Polar Front (Fig. 1; Mazloff et al., 2010). The archipelago is influenced by the Antarctic Circumpolar Current that flows eastward between 45°S and 65°S (Sallée et al., 2008; Solokov and Rintoul, 2009). The Antarctic Circumpolar Current and Southern Annular Mode (Gillett et al., 2006; Sallée et al., 2008) drives the Southern Westerly Winds which creates a humid and slightly cold subpolar climate. Today, the average annual precipitation is about 800 mm per year and the annual temperature is about 4.5°C at the scientific station Port-aux-Français (PAF) (i.e., at sea level). However, the precipitation amounts on the main island are affected by a strong W-E gradient due to a foehn effect on the eastern side of Cook Ice Cap (culminating at 1050 m asl and located on the western part of the archipelago), which constitutes a barrier to the dominant westerly winds. At Cook Ice Cap, the precipitation amount reaches 3150 mm per year at 250 m a.s.l. (Verfaillie et al., 2015). Altogether, the current climatic conditions still favor glacier preservation on Kerguelen

even at low elevations (*e.g.*, at ~400-1000 m asl). Indeed, the Kerguelen Archipelago still hosts currently the largest glaciated areas of the sub-Antarctic islands (552 km^2 in 2001; Berthier et al., 2009; Fig. 2). The largest ice body of the archipelago is the Cook Ice Cap located on the west side of the main island Grande Terre, which covered ~ 400 km^2 in 2020 (Verfaillie et al., 2021; Fig. 2). Other mountain glaciers can be found on the Rallier du Baty Peninsula, the Gallieni Peninsula and the Presqu'île de la Société de Géographie Peninsula (Fig. 2). However, recent studies on the archipelago showed that the atmospheric drying over Kerguelen since the 1960s, caused by the positive phase of the Southern Annular Mode, led to the shrinking of the glaciers, which are expected to completely disappear by 2100 CE (Berthier et al., 2009; Favier et al., 2016; Verfaillie et al., 2021).

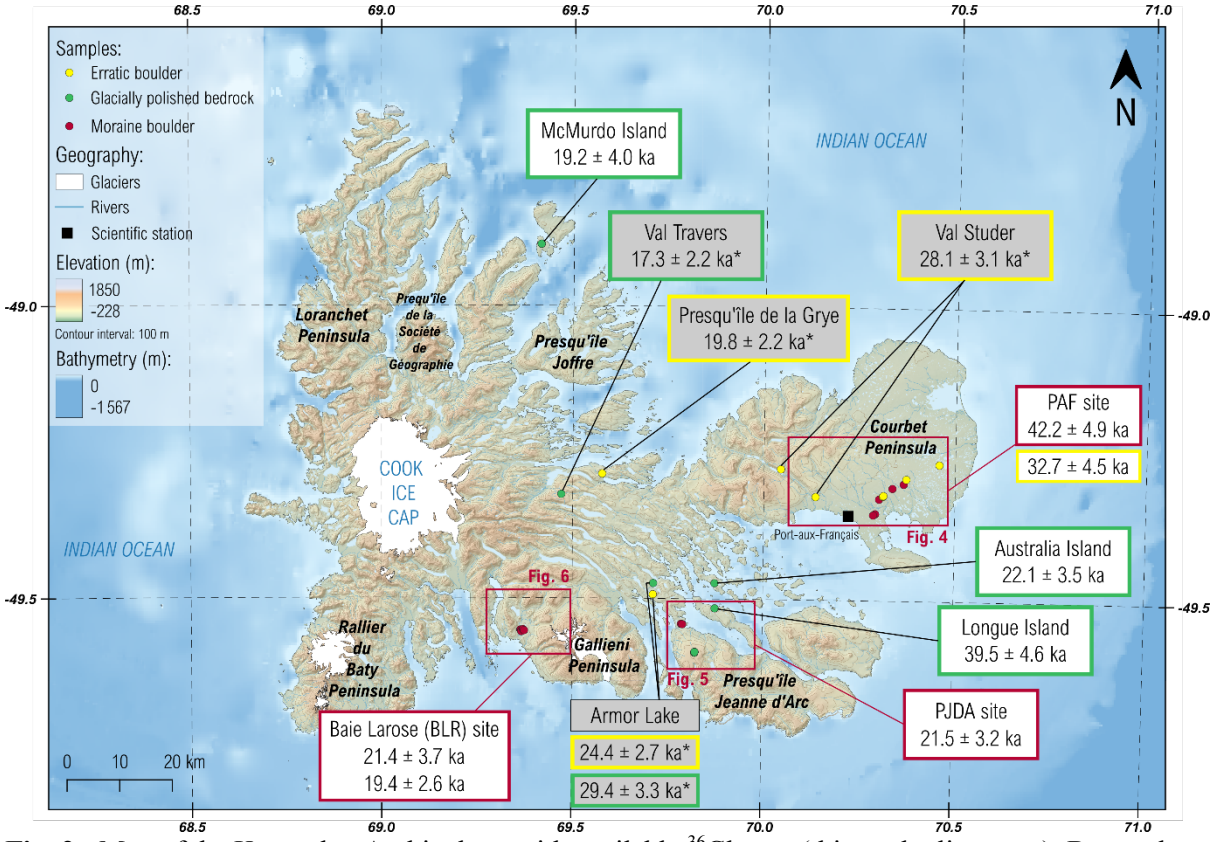

Fig. 2 - Map of the Kerguelen Archipelago with available ^{36}Cl ages (this study, literature). Boxes show arithmetic mean ^{36}Cl ages of samples of moraine boulders (red frames), erratic boulders (yellow frames) and glacially polished bedrock (green frames) from this study (white boxes) and previous literature (Grey boxes and asterisk; Jomelli et al., 2017, 2018; Charton et al., 2022) with their inferred total uncertainties. Three of the study areas are framed in red: Port-aux-Français (PAF) site, Port-Jeanne D'Arc (PJDA) site, and Baie Larose (BLR) site, for which geomorphological maps are presented in Figs. 4, 5 and 6, respectively. (data: Digital Elevation Model from NASA/METI/AIST/Japan

Spacesystems and U.S./Japan ASTER Science Team, 2019; glacier outlines from the GLIMS database (Raup et al., 2007)).

3. Methods

3.1. Sampling and study sites

Selecting sample sites on Kerguelen relies on logistic feasibility (*e.g.*, weather, boat cruise availability) as the entire archipelago is very difficult to reach. Also, glacio-geomorphic features are often hard to identify on aerial imagery and are only visible in the field.

Sample collection was carried out during a field campaign in 2017-2018. A total of 26 samples from glacially-polished bedrock and moraine boulders were collected for ^{36}Cl CRE dating (Table 1). We used a hammer and a chisel to extract the uppermost 2-3 cm flat and non-weathered moraine boulder and bedrock surfaces (*e.g.*, Fig. 3a, c). We recorded the geographic coordinates and elevations with a handheld GPS device and measured the topographic shielding in the field with a clinometer.

We targeted several sites around the archipelago that present glacio-geomorphological landforms expected to be older than the Holocene. For this study two following types of glacio-geomorphological features were dated: *(i)* moraine boulder samples, providing information on the extent and timing of a glacier being in equilibrium with climate at the end of a glacier advance or during a stillstand, hereafter referred to as culmination and *(ii)* glacially polished bedrock samples, informing on the timing of deglaciation during glacier retreat and the corresponding ice extent. While only features unambiguously formed by ice were sampled, the source areas of the glaciers cannot always be clearly identified, as described in the following paragraphs.

3.1.1. Moraine sampling sites

Moraines were investigated at the following three sites.

We first explored the surroundings of Port-aux-Français (PAF), which is the only scientific station on the archipelago, located in the eastern part of Courbet Peninsula (Fig. 2, 3 and 4). This area hosts features that are expected to document glacier fluctuations since MIS 3, based on the previous erratic boulders dated to 41.4 ± 4.4 ka (n=3) by Jomelli et al. (2018) (Fig. 4). The sampling site near PAF is, at first sight, rather flat and composed of Quaternary deposits with scattered erratic boulders lying on top (Fig. 3a, c). However, during this field campaign, moraine remnants, called here "PAF moraine" were identified. These moraine remains are about 20 m high and have an asymmetric cross profile with a gentle top and steep slopes, the distal slope being steeper than the proximal one (Fig. 3b). They are preserved over 300 m in length and have a north-south orientation. On top of these moraine remains, six large boulders were sampled at ~ 30-70 m asl. This PAF moraine was certainly deposited more than ~ 20 km east of a local paleo-glacier, with the assumed hilly accumulation area located on the '*Monts du Château*' (Fig. 4). Nowadays, no glaciers exist in this area. In between the PAF moraine and the assumed accumulation area of the paleo-glacier, some erratic boulders had already been dated (Jomelli et al., 2018) and may be associated with the same glacial advance period (Fig. 4).

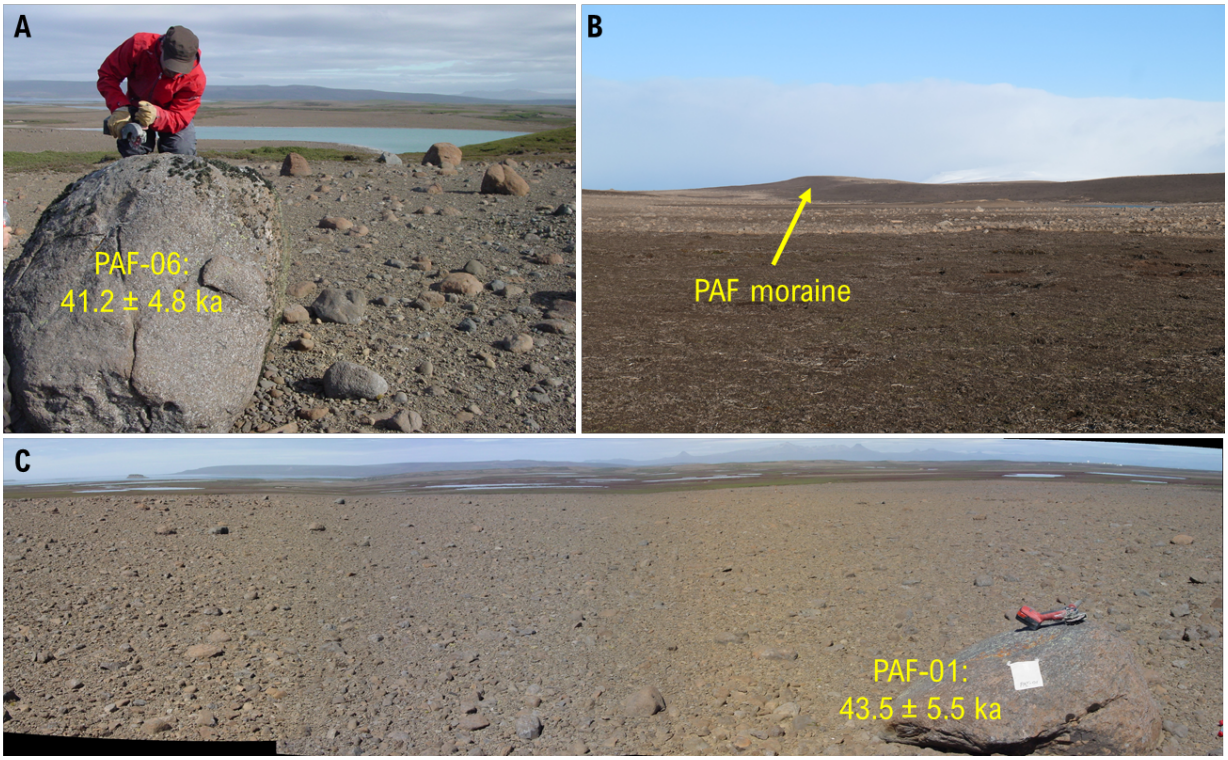

Fig. 3 - Photographs of sampled moraine boulders at the Port-aux-Français site, also displayed in Fig. 2 and 4. **A)** PAF-06 moraine boulder and the PAF moraine in the background. **B)** The PAF moraine. **C)** View of PAF moraine around PAF-01 moraine boulder. (Photos taken in 2018).

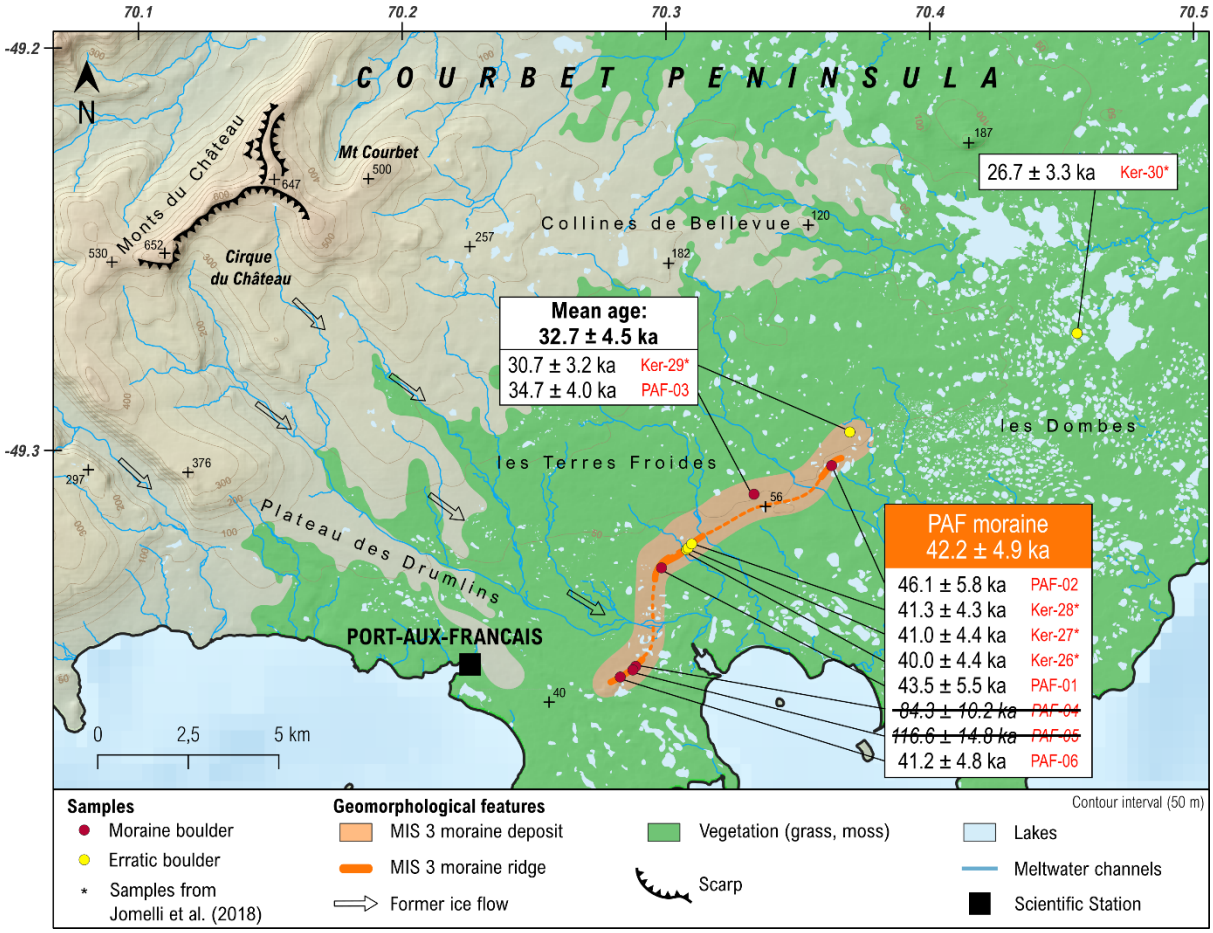

Fig. 4 - Glacial geomorphological map of the Port-aux-Français site. White boxes show new ^{36}Cl sample ages of moraine boulders and erratic boulders from Jomelli et al. (2018) with their inferred total uncertainties. Samples written in striked-through italic text are rejected as outliers and therefore excluded from the discussion. The arithmetic means for moraine boulder group (colored box) and glacially polished bedrock group (white box with black bold frame) are shown with their total uncertainties (*i.e.*, standard deviation, analytical and production rate uncertainties).

Then, we investigated the Port Jeanne D'Arc Peninsula (PJDA) located in the southeast of the archipelago (Figs. 2, 5). Here, the moraine remains also belong to disappeared local paleo-glaciers. Two moraine boulders were sampled on the isthmus of the peninsula at ~ 30 m asl. We assume that the former ice flowed southeast to northwest from paleo-glaciers located in the hilly center of the peninsula (~ 570 m asl) (Fig. 5).

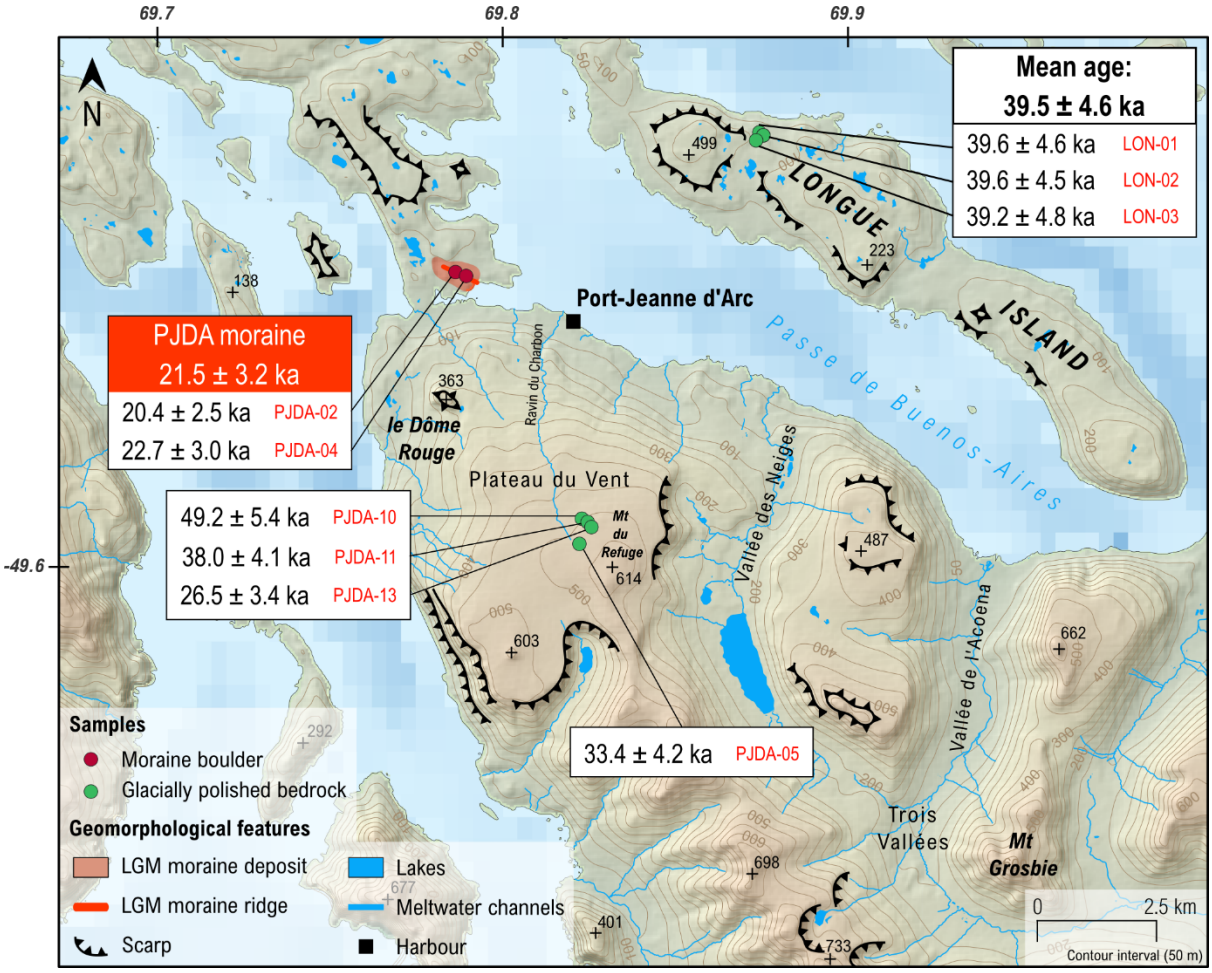

Fig. 5 - Glacial geomorphological map of the PJDA site. White boxes show new ^{36}Cl sample ages of moraine boulders and glacially polished bedrock with their inferred total uncertainties. The arithmetic means for moraine boulder group (colored box) and glacially polished bedrock group (white box with black bold frame) are shown with their total uncertainties (*i.e.*, standard deviation, analytical and production rate uncertainties).

Finally, we visited the Baie Larose site located south of the archipelago on the west side of the Gallieni Peninsula (Figs. 2, 6). This location is of particular interest since this peninsula is dominated by the highest peak of the archipelago, the stratovolcano Mt Ross (1850 m asl), around which several cirque glaciers still flow down to the valley but remain poorly documented so far (*e.g.*, '*Glacier de Casse Déserte*', '*Glacier de Bonne Pierre*'; Fig. 6). Moreover, the already partially surveyed mountain glaciers located on the eastern slope of Mt Ross are largely debris-covered (Charton et al., 2021), whereas glaciers located on its western flank are mostly debris-free. Deposited by these debris-free glaciers, two moraines were

targeted for sampling. These moraines were most probably formed by a local glacier on the northwestern flank of the volcano at ~ 8 km from the current glacier front and at ~ 2 km from the sea (Figs. 6, 7). The two moraines are separated by a horizontal distance of ~ 390 m. On the inner B2 moraine (Fig. 7b), two samples were extracted from moraine boulders at ~ 115 m asl, and five samples were taken on the outer B1 moraine at ~80 m asl (Fig. 7a, c).

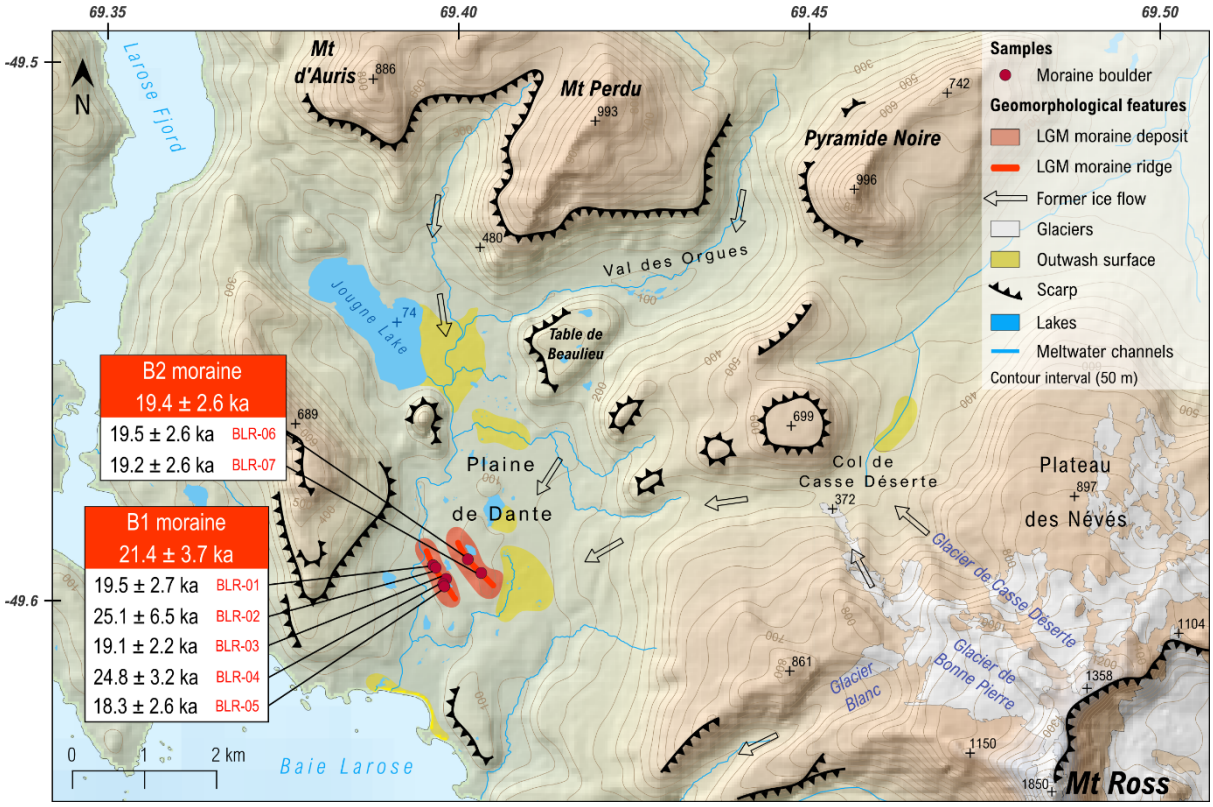

Fig. 6 - Glacial geomorphological map of the Baie Larose site. White boxes show new ^{36}Cl sample ages of moraine boulders with their inferred total uncertainties. The arithmetic means for moraine groups are shown in colored boxes with their total uncertainties (*i.e.*, standard deviation, analytical and production rate uncertainties).

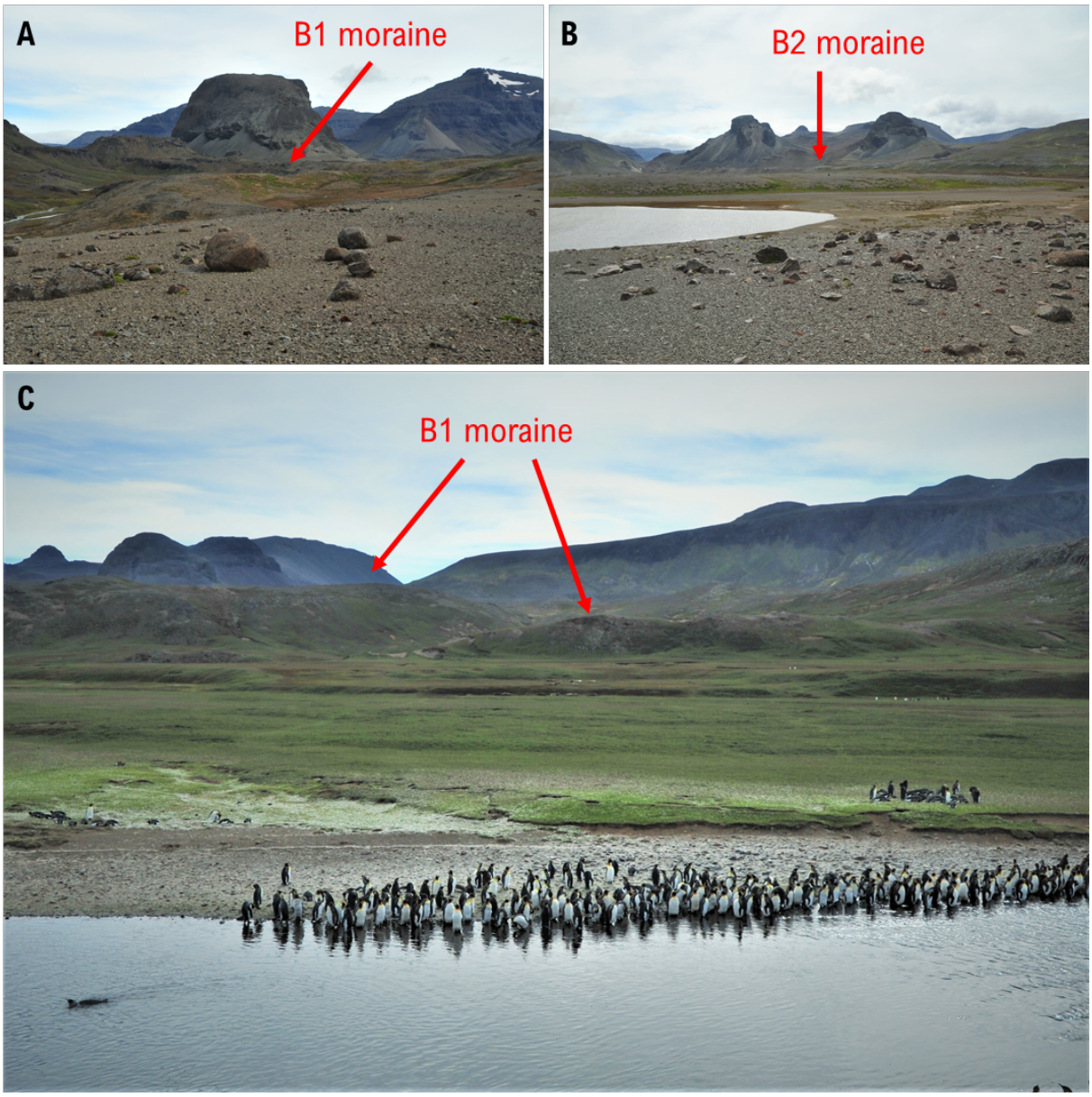

Fig. 7 - Photographs of moraines at Baie Larose site. **A)** B1 (outer) moraine at Baie Larose site. **B)** B2 (inner) moraine at Baie Larose site. **C)** B1 moraine from the sea.

3.1.1. Glacially polished bedrock sampling sites

In addition to the moraines at these three sites, we collected samples from glacially polished bedrock surfaces in four distal areas east- and northward from the Cook Ice Cap (Fig. 2). Two of the sites were located on two small islands: Australia Island and Longue Island. These islands located south of the Courbet Peninsula and in total five samples were extracted from

glacially polished bedrock. Two samples were taken on Australia Island at 62 m asl and three others on Longue Island at 110 m asl (Fig. 2).

The third site was on the PJDA Peninsula, between the supposed accumulation area of the paleo-glacier and the PJDA moraine deposition. Four glacially polished bedrock surfaces were sampled: one at low elevation (260 m asl) and three at higher elevation (480 m asl) (Fig. 5).

The last site was on McMurdo Island, a very isolated area located in the north of the archipelago. We extracted two samples from glacially polished bedrock at ~ 151 m asl (Fig. 2).

3.2. *In situ* ^{36}Cl laboratory analysis

The basaltic whole-rock samples were processed for ^{36}Cl extraction at LN_2C (CEREGE, France) according to routine procedures using the same methods as in the previous studies undertaken on Kerguelen (Jomelli et al., 2017, 2018; Charton et al., 2020, 2022; Verfaillie et al., 2021). $^{36}Cl/^{35}Cl$ and $^{35}Cl/^{37}Cl$ ratio measurements were performed at the ASTER AMS national facility (CEREGE, France) after normalization to the inhouse standard SM-CL-12, using an assigned value of 1.428 (± 0.021) x 10^{-12} for the $^{36}Cl/^{35}Cl$ ratio (Merchel et al., 2011) and assuming a natural ratio of 3.127 for the stable ratio $^{35}Cl/^{37}Cl$. ^{36}Cl CRE ages were calculated with the Schimmelpfennig et al. (2009) Excel spreadsheet, assuming no denudation or snow cover and using the time-invariant "St" scaling scheme (Stone, 2000). The chemical composition of the samples used for the calculation are displayed in Tables 2 and 3. Consistent with the earlier studies on Kerguelen, the following ^{36}Cl sea level high latitudes (SLHL) production rates were used for the calculations: 42.2 ± 4.8 atoms of $^{36}Cl\ (g\ Ca)^{-1}\ yr^{-1}$ for Ca spallation (Schimmelpfennig et al., 2011), 148.1 ± 7.8 atoms of $^{36}Cl\ (g\ K)^{-1}\ yr^{-1}$ for K spallation (Schimmelpfennig et al., 2014), 13 ± 3 atoms of $^{36}Cl\ (g\ Ti)^{-1}\ yr^{-1}$ for spallation of Ti (Fink et al., 2000), 1.9 ± 0.2 atoms of $^{36}Cl\ (g\ Fe)^{-1}\ yr^{-1}$ for Fe spallation (Stone et al., 2005), and 696 ± 185 neutrons $(g\ air)^{-1}\ yr^{-1}$ for the rate of epithermal neutron production from fast neutrons in

the atmosphere at the Earth/atmosphere interface (Marrero et al., 2016). We applied a value of 160 g cm^{-2} for the high-energy neutron attenuation length and 2.4 g cm^{-3} for the bulk rock density. The resulting ^{36}Cl ages with their associated 1 σ uncertainties (*i.e.,* the total uncertainties which take into account the analytical and production rate uncertainties) and their analytical uncertainties in brackets are listed in Table 4. Moraine ages and grouped bedrock ages result from the arithmetic means of the individual sample ages that successfully pass a Chi^2 test, calculated with their analytical uncertainties (Ward and Wilson, 1978). In the main text and on the figures, ages are reported with their total uncertainties.

3.3. Compilation of CRE moraine boulder ages for comparison with other moraine chronologies from the southern mid-latitudes

To get a better understanding of glacier fluctuations in the southern mid-latitudes, we performed a compilation of CRE moraine boulder ages based on version 1 of the alpine informal cosmogenic-nuclide exposure-age database (ICE-D database; now replaced by https://version2.ice-d.org/alpine/). All the ^{10}Be, ^{26}Al and ^{3}He CRE ages gathered within ICE-D are recalculated with the online exposure age calculator v3 (http://hess.ess.washington.edu/; after Balco et al., 2008) using the same parameters for all the nuclides, which are the St scaling method (Stone, 2000) chosen for this study, the ERA40 reanalysis atmosphere model (Uppala et al., 2005) and the GLOPIS-75 magnetic field reconstruction (Laj et al., 2004). Regarding the production rates, we chose the default data set calibrated from the CRONUS-Earth primary calibration data sets of Borchers et al. (2016) for ^{10}Be and ^{26}Al in quartz and ^{3}He in pyroxene/olivine.

We also recalculated four ^{36}Cl CRE ages (n=4) from Marion Island (Rudolph et al., 2020) with the Schimmelpfennig et al. (2009) Excel spreadsheet using the same parameters and methods as explained above for the Kerguelen ^{36}Cl CRE ages calculation.

While compiling, two criteria were considered: *(i)* we only included CRE-dated moraine boulder ages, and *(ii)* we considered a moraine only if it was dated with at least two CRE boulder ages that successfully passed a Chi^2 test. For CRE age pools successfully passing the Chi^2 test, an arithmetic mean age and standard deviation of the landform was calculated.

All the compiled ^{10}Be, ^{26}Al, ^{36}Cl and ^{3}He CRE moraine ages are presented in Supplemental Tables 1, 2 and 3 calculated with the St (Stone, 2000) scaling scheme. They are reported with their standard deviation.

4. Results

We obtained 26 new ^{36}Cl CRE ages from the six sites on Kerguelen. We first present in chronological order the results of moraine boulder samples collected on the PAF site, PJDA site and Baie Larose site and then those from glacially polished bedrock surfaces at Longue Island, PJDA Peninsula, Australia and McMurdo islands.

4.1. Moraine boulders ^{36}Cl CRE ages

At the PAF sampling site, the five moraine ridge boulders PAF-01, -02, -04, -05 and -06 yield ^{36}Cl ages of 43.5 ± 5.5 ka, 46.1 ± 5.8 ka, 84.3 ± 10.2 ka, 116.6 ± 14.8 ka and 41.2 ± 4.8 ka, respectively (Table 4, Fig. 4). PAF-04 and -05 are probably affected by nuclide inheritance and are rejected as outliers. Due to their close location, these samples from the moraine ridge can morphologically be associated with some of the erratic boulders already published in Jomelli

et al. (2018) and may thus be associated with the same glacial event. These erratic boulders are Ker-26, -27 and -28, which gave ages of 39.3 ± 3.6 ka, 40.4 ± 3.6 ka and 39.4 ± 3.5 ka, respectively (Jomelli et al., 2018). Taken together, the six samples PAF-01, -02, and -06, Ker-26, -27 and -28 yield an arithmetic mean age of 42.2 ± 4.9 ka (n=6). This mean age confirms the age of the three erratic boulders from this location previously dated by Jomelli et al. (2018) at 41.4 ka ± 4.4 ka. Boulder PAF-03 is located on the till inboard of the PAF moraine ridge, and gives an age of 34.7 ± 4.0 ka. This boulder has a stratigraphically similar position as the previously dated boulder Ker-29 that gave an age of 30.7 ± 3.2 ka (Jomelli et al., 2018). Altogether the arithmetic mean and total uncertainty of these two boulders are 32.7 ± 4.5 ka (n = 2).

On the PJDA Peninsula, samples PJDA-02 and -04, from the PJDA moraine give consistent ages of 20.4 ± 2.5 ka and 22.7 ± 3.0 ka, respectively, and yield a mean age of 21.5 ± 3.2 ka (n = 2) (Table 4, Fig. 5).

At the Baie Larose site, the ^{36}Cl ages from the base of Mt Ross BLR-01, -02, -03, -04 and -05 of the outermost (oldest) B1 moraine are 19.5 ± 2.7 ka, 25.1 ± 6.5 ka, 19.1 ± 2.2 ka, 24.8 ± 3.2 ka and 18.3 ± 2.6 ka, respectively (Table 4, Fig. 6). The arithmetic mean and total uncertainty of B1 moraine are 21.4 ± 3.7 ka (n = 5). On the innermost (youngest) B2 moraine, samples BLR-06 and -07 give ^{36}Cl ages of 19.5 ± 2.6 ka and 19.2 ± 2.6 ka, with a mean age of 19.4 ± 2.6 ka (Table 4, Fig. 6). The nominal moraine mean ages are in agreement with their stratigraphic position, though it is noteworthy that the seven individual ages from both B1 and B2 moraines are indistinguishable.

4.2. Glacially polished bedrocks ^{36}Cl CRE ages

The three bedrock surface samples extracted on Longue Island, LON-01, -02 and -03, yield consistent ages of 39.6 ± 4.6 ka, 39.6 ± 4.5 ka and 39.2 ± 4.8 ka, respectively. The arithmetic

mean age and total uncertainty of the bedrock surfaces at Longue Island are 39.5 ± 4.6 ka (Table 4, Fig. 5).

On the PJDA Peninsula, glacially polished bedrock samples located ~6 km SE' of the moraine give ^{36}Cl ages of 33.4 ± 4.2 ka at lower elevation (PJDA-05), and 49.2 ± 5.4 ka, 38.0 ± 4.1 ka and 26.5 ± 3.4 ka at higher elevation (PJDA-10, -11 and -13) (Table 4, Fig. 5). These latter three ages are inconsistent with each other according to the Chi^2 test. Also, though the origin of the ice flow remains unclear, the four glacially polished bedrock samples seem to be inboard of the PJDA moraine. Thus, it is most likely that these ages are overestimated for so far inexplicable reason. Indeed, they should be younger than ~ 21 ka.

Bedrock surface samples from Australia Island, AUS-02 and -05, give ages of 20.8 ± 2.6 ka and 23.4 ± 3.2 ka, respectively. Together these samples yield a mean bedrock surface age of 22.1 ± 3.5 ka (Table 4, Fig. 2).

Finally, at the McMurdo Island sampling site, the ^{36}Cl ages of the two bedrock surface samples are 21.5 ± 2.7 ka and 17.0 ± 2.2 ka, respectively. The arithmetic mean age of these two samples at McMurdo Island is 19.2 ± 4.0 ka (Table 4, Fig. 2).

5. Discussion

5.1. Late Pleistocene glacier chronologies on Kerguelen

The 26 new ^{36}Cl ages obtained from moraine boulders and glacially polished bedrock samples at several locations on the Kerguelen Archipelago help refine Late Pleistocene glacier fluctuations (Jomelli et al., 2018; Charton et al., 2022; Fig. 2). The oldest evidence of glacier culmination on the archipelago is shown by the PAF moraine, which was deposited at 42.2 ±

4.9 ka (n=6). So far, this moraine is the only dated glacio-geomorphological feature that attests to a large glacier advance or stagnation during the MIS 3 period. The PAF moraine was emplaced at ~ 20 km from the assumed paleo-accumulation area of the former glacier near Mont du Château (Fig. 4).

Another extensive glacier advance or stagnation happened during the gLGM, as suggested by moraines in two other locations on the archipelago. One is a moraine dated at 21.5 ± 3.2 ka (n=2) located on the Port Jeanne D'Arc Peninsula (PJDA) (Fig. 5). The other moraine site is Baie Larose on the Gallieni Peninsula, where the outer B1 moraine is dated at 21.4 ± 3.7 ka (n=5) and the inner B2 moraine was deposited at 19.4 ± 2.6 ka (n=2) (Fig. 6). Hitherto, this is the first time that gLGM glacier advances are evidenced in the Kerguelen Archipelago and it seems this event was probably synchronous at the archipelago scale. The PJDA moraine and the set of moraines at Baie Larose were emplaced at ~ 8-9 km from the accumulation area of their respective glaciers (Figs. 5, 6). In addition, the moraines are located very close to the shoreline (less than ~ 2 km), suggesting that glacio-geomorphological features of advances pre-dating the gLGM at these sites are nowadays underwater.

In between these two extensive glacier culminations, *in situ* ^{36}Cl dating of glacially polished bedrock surfaces at several places on the islands provide new knowledge of the history of deglaciation since the maximum glacier extent on the archipelago (Fig. 2). The oldest CRE ^{36}Cl bedrock ages of ~ 39.5 ka are located on the eastern side of the archipelago on Longue Island, indicating a long period free of ice between MIS 3 and probably nowadays at this relatively low elevation location (~ 110 m asl) (Fig. 5). Assuming that both local mountain and ice cap glaciers experienced events of greater extent at ~ 42.2 ka that covered most of the archipelago, these older bedrock surfaces from Longue Island suggest that the culminations were rapidly followed by a period of deglaciation. It is very likely that since shortly after the MIS 3 glacier

393 expansion, this part of the archipelago has never been covered by ice again. Indeed, we suppose
394 that subsequent local glacier extents as large as the MIS 3 culmination can be excluded or if
395 larger local glacier advances occurred, they did not erode enough rock surfaces to remove the
396 entire previously accumulated ^{36}Cl inventory. Other new bedrock surfaces located on the
397 eastern part of the archipelago, on Australia Island and PJDA Peninsula, provide ^{36}Cl CRE ages
398 varying from ~ 49.2 ka to ~ 22.1 ka and covering a similar age span as five bedrock surfaces
399 at Armor Lake (~ 32 ka to ~ 25 ka) as well as two erratic boulders at Armor Lake (~ 24 ka),
400 five erratic boulders in Val Studer (~ 31 ka to ~ 24 ka) and two erratic boulders in Courbet
401 Peninsula (PAF site; ~ 30 ka to ~ 26 ka) (Jomelli et al., 2018) (Figs. 2, 5). Considering glacier
402 culminations with large extents during MIS 3 (~ 42.2 ka) and MIS 2 (gLGM; ~ 21-19 ka) on
403 the archipelago, these bedrock ages attest to a general trend of deglaciation in between these
404 two events. However, the dispersed bedrock and erratic boulder ages at the PJDA, PAF, Amor
405 Lake and Val Studer sites (Fig. 2) suggest a complex history of exposure with probably
406 alternating ice-free/ice-covered periods and non-uniform erosion. In addition, these bedrock
407 surfaces are located at varying elevations ranging from ~ 60 m asl to ~ 480 m asl, and the
408 geometry of the paleo-ice cover has not yet been reconstructed in this complex setting of fjords
409 and islands surrounded by higher-elevation topography. Thus, a specific chronology of glacier
410 fluctuations for individual ice bodies in this area is hard to establish. Altogether, these bedrock
411 and erratic boulder ages confirm a general deglacial trend on the eastern part of the archipelago
412 from ~ 42.2 ka to 21-19 ka, in agreement with the scenarios proposed earlier (Jomelli et al.,
413 2017, 2018).

414 Subsequently, younger bedrock surfaces located on the McMurdo Island on the north of Cook
415 Ice Cap show apparent ages of ~ 19.2 ka (Fig. 2). It implies that after the glacier culmination
416 during the gLGM, another period of deglaciation was initiated rapidly. In addition, it is most
417 likely that glaciers never readvanced to this position but remained relatively confined until they

418 disappeared (Fig. 2). These ages are consistent with a bedrock sample from Val Travers valley
419 that gave an age of ~ 17.3 ka (Charton et al., 2022) and an erratic boulder dated at ~ 19.8 ka
420 from Presqu'île de la Grye (Jomelli et al., 2017), that suggested a deglaciation process (Fig. 2).
421 Altogether, the combined ages of glacially polished bedrock and erratic boulder samples from
422 the gLGM - Late Glacial transition indicate that glaciers started to retreat shortly after the
423 gLGM glacier advances. Finally, the last Pleistocene glacier advances occurred on Kerguelen
424 during Heinrich Stadial 1 (17.5 - 14.7 ka; Rasmussen et al., 2014) and the Antarctic Cold
425 Reversal (14.5 - 12.9 ka) events (Jomelli et al., 2017, 2018; Charton et al., 2020, 2022).

426 **5.2. Comparison with other moraine chronologies in the southern mid-latitudes**

427 Our new ^{36}Cl CRE age dataset underlines an advance of mountain glaciers on Kerguelen (49°S,
428 69°E) during MIS 3 (42.2 ± 4.9 ka; moraine deposited at ~ 20 km from the accumulation area)
429 that was greater than during the gLGM (21.5 ± 3.2 ka, at 21.4 ± 3.7 ka and at 19.4 ± 2.6 ka;
430 moraines deposited at ~ 8-9 km from the accumulation area). The large uncertainties in the ^{36}Cl
431 age of the PAF moraine preclude a millennial-scale comparison with other glacier records. We
432 therefore focus here on whether glacier culminations during the time range ~ 47-37 ka with
433 extents beyond the gLGM advances was a common phenomenon in the southern mid-latitude
434 regions. Indeed, at the study site in the sub-Antarctic sector that is closest to Kerguelen, Skua
435 Ridge site on Marion Island (46°S, 37°E), moraines were dated with ^{36}Cl at 40.0 ± 4.1 ka and
436 at 36.1 ± 3.8 ka (Rudolph et al., 2020; see method section for the ^{36}Cl ages recalculation). The
437 moraines at the following sites were all dated with the ^{10}Be CRE dating method. In New
438 Zealand (43°S, 170°E), the Pukaki glacier also exhibits several lateral moraines during this
439 period, *i.e.*, at 43.0 ± 1.3 ka, 41.1 ± 1.9 ka and 41.1 ± 1.1 ka (Kelley et al., 2014; Strand et al.,
440 2019). In South America, glaciers in almost the entire Patagonian latitudinal belt experienced
441 culminations of large extent during this time span. For instance, moraine ages in the Central

Andes show an overall consistency with the timing of glacier culmination on Kerguelen, in particular in Cordon de Dona Rosa (30°S, 70°W) where the glacier culminated at 37.8 ± 2.4 ka (Zech et al., 2007), and in the Rucachoroi Valley where the glacier advanced at 41.3 ± 1.6 ka (Zech et al., 2011). Finally, in the Southern Patagonian Icefield (50-51°S, 71-72°W), moraines are dated to 37.2 ± 1.1 ka and 46.4 ± 2.7 ka in Torres del Paine (Garcia et al., 2018) and 46.6 ± 1.5 ka in the Ultima Esperanza Lobe (Garcia et al., 2018). These moraine chronologies are supported by CRE dated glacial features at other sites. Very close to the Ultima Esperanza Lobe, in Cerro Benítez, erratic boulders deposited during ice melting are dated at a minimum age of 35.1 ± 1.6 ka (Girault et al., 2022). And further south (53-54°S), the glacial limit of the Río Cullen of the former Bahía Inútil–San Sebastián ice lobe on Tierra del Fuego gives an age of ~ 45.6 ka based on cosmogenic ^{10}Be and ^{26}Al dating of glacial outwash sediments (Darvill et al., 2015). In conclusion, it seems that the Kerguelen MIS 3 glacier maxima at 42.2 ± 4.9 ka may have been in phase with the other studied localities in the southern mid-latitudes, although the uncertainties associated with the PAF moraine age dating are high (Fig. 8g, h).

Regarding the gLGM glacier culminations observed on Kerguelen at 21.5 ± 3.2 ka (PJDA moraine), at 21.4 ± 3.7 ka (B1 moraine) and at 19.4 ± 2.6 ka (B2 moraine), it is noteworthy that evidence of gLGM advances is missing so far on any other sub-Antarctic islands, such as on Marion Island. However, the Alpine ICE-D dataset (^{10}Be, ^{26}Al and ^{3}He CRE ages; Supplementary Tables 1, 2, 3) provides information on numerous moraines dated within this period in Australia and Tasmania ($n_{moraines}$=5; *e.g.*, Kiernan et al., 2004), in New Zealand ($n_{moraines}$=23; *e.g.*, Putnam et al., 2013; Denton et al., 2021; Tielidze et al., 2022) and Patagonia ($n_{moraines}$=21; *e.g.*, Kaplan et al., 2007; Leger et al., 2021; Çiner et al., 2022). To sum up, Kerguelen glacier culminations during the gLGM are synchronous with the global event that also occurred throughout the southern mid-latitudes (Fig. 8 g, h).

5.3. Unresolved Late Pleistocene climatic conditions on Kerguelen

^{36}Cl dating of 26 moraine boulders and glacially polished bedrock samples allowed us to refine our knowledge on glacier evolution on Kerguelen during the Late Pleistocene, in particular since ~ 42.2 ka and until the end of the gLGM. Based on this updated glacier chronology, we now investigate regional climate conditions that may be responsible for such glacier fluctuations on the archipelago. In contrast to the differing trend at a multi-millennial timescale of the glacier evolution in the southern mid-latitudes during the Holocene (Charton et al., 2022), it seems that glaciers during periods around ~ 42.2 ka and ~ 21-19 ka, may be synchronous in all these regions considering the high uncertainties of ^{36}Cl ages (Fig. 8g, h).

The MIS 3 period is characterized by strong climate variability punctuated by several millennial-events such as Heinrich stadials (HS), *i.e.*, cold periods over Greenland and the North Atlantic, and Dansgaard Oeschger events (DO), *i.e.*, abrupt Greenland warming (NGRIP, 2004; Menviel et al., 2020; Fig. 8a), as well as their corresponding Southern Hemisphere Antarctic Isotope Maximum (AIM) (EPICA, 2006) (Fig. 8). During the MIS 3 period, the oldest glacio-geomorphological evidence of glacier activity on Kerguelen is a moraine resulting from glacier culmination at ~ 42.2 ka. Thus, it raises the question of whether this glacier culmination resulted from a high- (*i.e.*, centennial to millennial timescale such as the Northern Hemisphere HS) or low-frequency climate driver. So far, the relatively high uncertainty associated with the moraine age prevents us from a clear assignment to a specific climate event during MIS 3, in particular as several climatic events occurred during the time span of the uncertainties (~47-37 ka). These climate events are five AIM/DO events (8, 9, 10, 11 and 12; Fig. 8a, b; NGRIP, 2004; EPICA, 2006), the HS4 event (Fig. 8a; NGRIP, 2004) and four cold peaks (~37 ka, ~41 ka, ~43 ka and ~45 ka, Fig. 8b) recorded in the WDC ice core from the West Antarctic Ice Sheet (WAIS Divide Project Members, 2015). If the ~ 42.2 ka moraine on the Kerguelen

Archipelago cannot be associated with one of the cold high-frequency climatic events, we then explore the hypothesis that this glacier maximum was driven by low-frequency climate conditions. A study on the current glacier evolution on Kerguelen showed that surface air temperature and sea surface temperatures (SSTs) are correlated (Favier et al., 2016). Therefore, we assume that paleo SST data should be more representative of the local glacier-driving climate than atmospheric temperatures from Antarctic ice cores. Here, we discuss the relevance of reconstructed paleo SSTs from the core MD11-3353 (50°34.02′S, 68°23.13′E; Fig. 8d) located southwest of Kerguelen (Civel-Mazens et al., 2021). Besides, this marine core makes it also possible to document latitudinal changes in the position of the oceanic fronts (that drove the Southern Westerly Winds). Although this local record does not document the period before and around 42.2 ka, relatively cold temperatures are reported around 41-40 ka, so that we can speculate that temperatures were rather cold during the emplacement of the 42.2 ± 4.9 ka moraine on the Kerguelen Archipelago. During MIS 3, SSTs from cores (only shown in this study is core MD11-3353 in Fig. 8d) around Kerguelen suggest a more northward position of the Antarctic Circumpolar Current fronts compared to their present location, in particular the Antarctic Polar Front would have been located north of the Kerguelen Plateau (Civel-Mazens et al., 2021). This northward migration of the Antarctic Polar Front implies long-term glacial conditions around Kerguelen that may have favored the glacier expansion observed at MIS 3. Such cold SSTs conditions were also reported around 45-40 ka (Jomelli et al., 2018) from the Cape Basin 1089/TN057 sediment core (41°S), located on the northwest of Kerguelen in the Atlantic sector of the Southern Ocean (Pahnke and Sachs, 2006)

Regarding the gLGM advance on Kerguelen, SSTs from the marine core MD11-3353 interestingly show conditions that are approximately as cold at ~42.2 ka as at ~21-19 ka, indicating that hydrological fronts were also located north of the Kerguelen Plateau during the gLGM (Civel-Mazens et al., 2021). However, this marine record does not provide plausible

explanations for the larger glacier expansion at MIS 3 than during the gLGM on Kerguelen, as local SST reconstructions show no substantial temperature variation between the two investigated periods. Last but not least, an increase of SSTs in core MD11-3353 (Fig. 8d) from ~ 18 ka implies that the Antarctic Polar Front rapidly migrated southward (Civel-Mazens et al., 2021), which may explain the deglacial trend initiated at that time on Kerguelen.

As long-term temperature variations do not change significantly between ~42.2 ka and ~21-19 ka, we suppose that precipitations also triggered glacier culmination on Kerguelen. Indeed, previous studies on the archipelago suggest that glaciers are highly sensitive to precipitation changes influenced by the position of the Southern Westerly Winds (*e.g.*, Favier et al., 2016). As precipitation may be a key driver of the investigated glaciers, we explore the possible correspondence between the reconstruction of paleo-precipitation and the glacier evolution on Kerguelen. Unfortunately, terrestrial paleo-precipitation records are rare in the sub-Antarctic sector, in particular on such timescale. Yet, growth rate and stable isotope ($\delta^{18}O$, $\delta^{13}C$) profiles from a stalagmite (HW3) recovered from Hollywood Cave (41°57′S, 171°28′E; 130m asl) in New Zealand, allow a centennial-scale investigation of the Southern Westerly Winds paleointensity and thus precipitation amounts between 73 and 11 ka for the ~ 41° latitudes (Whittaker et al., 2011; Fig. 8f). Speleothem growth rate increased for several millennia around ~ 42.2 ka, which indicates wetter conditions in favor of glacier expansion. Speleothem growth rate also peaked briefly at ~ 22-21 ka, but quantitatively twice that amount at ~ 42.2 ka. We suggest that the shortly enhanced precipitation combined with the cold temperatures may have triggered the ~ 21.5 ka glacier advance in Kerguelen, but the rapidly following dryer conditions during the gLGM may have prevented glaciers on Kerguelen from advancing as far as their previous MIS 3 extents. Still, due to the geographically remote location of this speleothem climate record, correlating its interpretation to Kerguelen glacier fluctuations remains speculative. However, it is noteworthy that in a transient simulation of the last glacial period

(Menviel et al., 2011; 2014) a decreasing trend in precipitation amount is simulated around Kerguelen from ~38 ka to the gLGM, whereas an increasing trend is simulated from ~ 47-38 ka (Fig. 8e), which may also support our hypothesis.

It remains also challenging to unravel the climatic conditions that drove the glacier evolution in the other mid-latitude regions, and - given their similarity - to understand whether or not all glaciers were driven by the same large-scale mechanisms. The authors of several studies from both New Zealand and Patagonia noticed a discrepancy between southern summer insolation change and glacier change (Kelley et al., 2014; Doughty et al, 2015; Garcia et al., 2018; Strand et al., 2019). They considered it unlikely that summer insolation had a significant effect on glacier evolution, as it varied from high (at ~45 ka), mid (at ~19 ka) to low (at ~60 ka, ~30 ka) intensity during the MIS 3 period and was not in phase with glacier maxima (Kelley et al., 2014; Garcia et al., 2018; Strand et al., 2019; Fig. 8c). Similar to our observations from the Kerguelen Archipelago, Doughty et al. (2015) evidence glacier maxima in New Zealand in phase with regional SST changes from the Southern Ocean. Lastly, Garcia et al. (2018) show that multi-millennial glacier culminations in both Patagonia and New Zealand are closely teleconnected to the Antarctic climate, in particular because most glacial maxima occurred synchronously with cold periods recorded in Antarctic ice cores. Nevertheless, these authors argue that this concordance is not sufficient to explain the advance of glaciers being larger during MIS 3 than during the gLGM, as is recorded at numerous sites in the southern mid-latitudes, including the Kerguelen Archipelago.

To sum up, climatic drivers responsible for glacier fluctuations on Kerguelen from the MIS 3 period to the end of the gLGM remain puzzling. It seems that there was a long-term mid to high southern latitude cooling broadly in phase that may partly explain the Late Pleistocene glacier maxima on the archipelago at ~42.2 ka and ~21-19 ka, as well as in New Zealand and

564 Patagonia (Garcia et al., 2018). However, so far, none of the climate proxies explored in this
565 study provide a robust explanation for the larger MIS 3 glacier culmination on Kerguelen and
566 elsewhere in the southern mid-latitudes. Here, we hypothesize that temperature alone cannot
567 explain glacier expansion and retreat on the archipelago and that precipitation changes may
568 have created a tipping point that superimposed on the impact of temperature variations. Indeed,
569 the larger MIS 3 glacier advance was certainly caused by a higher amount of precipitation that
570 compensated for comparable to those documented during the gLGM temperatures conditions,
571 while limited amounts of precipitation may have led to smaller glacier extent during the gLGM.
572 To better understand the climatic mechanisms that influenced glacier variations in the
573 Kerguelen Archipelago, additional research on the regional paleoclimatology is needed.

574

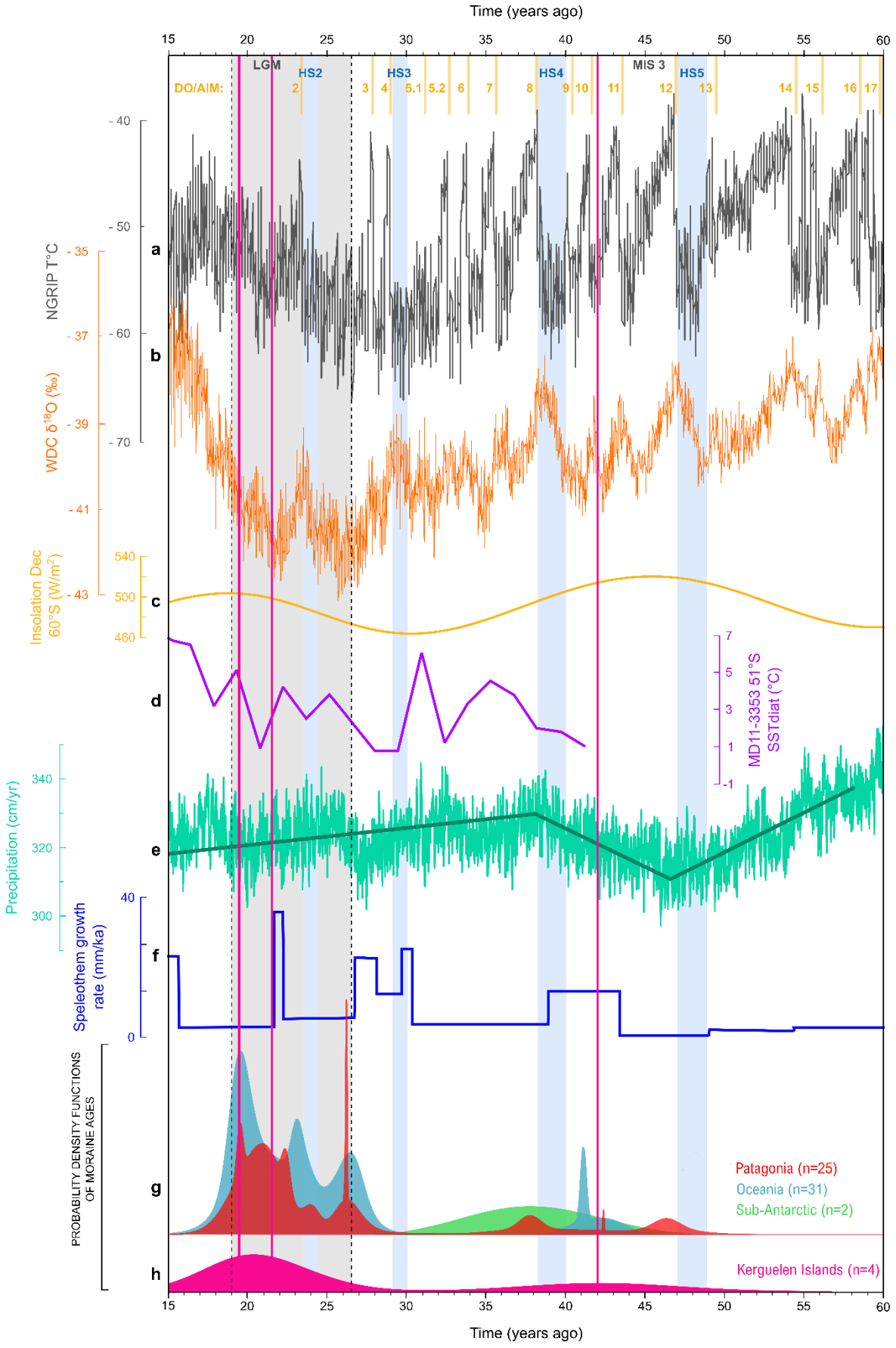
Time (years ago)
LGM
HS2
HS3
HS4
HS5
MIS 3
DO/AIM:
NGRIP T°C
WDC δ18O (‰)
Insolation Dec 60°S (W/m2)
MD11-3353 51°S SSTdiat (°C)
Precipitation (cm/yr)
Speleothem growth rate (mm/ka)
PROBABILITY DENSITY FUNCTIONS OF MORAINE AGES
Patagonia (n=25)
Oceania (n=31)
Sub-Antarctic (n=2)
Kerguelen Islands (n=4)
a
b
c
d
e
f
g
h

575

Fig. 8 - Comparison of Kerguelen paleoglacier records with Artic, Antarctic and southern mid-latitude climatic proxies. Proxies for Northern Hemisphere atmospheric temperature fluctuations are **a.** T°C (black curve) from NGRIP (Johnsen et al., 2001) and for the Southern Hemisphere **b.** $\delta^{18}O$ (orange curve) from the WDC ice core in West Antarctica (WAIS Divide Project Members, 2015). **c.** are the summer (December) insolation changes at 60°S (Berger and Loutre, 1991). **d.** is the reconstructed SSTs from the MD11-3353 core (51°S; Civel-Mazens et al., 2021). **e.** Precipitation changes around Kerguelen from the LOVECLIM transient simulation (Menviel et al., 2011; 2014). **f.** is the growth rate from a stalagmite (HW3) recovered from Hollywood Cave (41°57′S, 171°28′E; 130 m above sea level) in New Zealand (Whittaker et al., 2011). Also shown are **g.** the CRE moraine age probability density distributions with their standard deviation during the investigated period from southern mid-latitude glaciers excluding those on Kerguelen, and **h.** the new ^{36}Cl CRE moraine age probability density distributions with their inferred full uncertainties from Kerguelen (pink vertical bands are the arithmetic mean ages of moraines). Vertical grey band corresponds to the Last Global Maximum (Clark et al., 2009), blue bands to Heinrich Stadials (NGRIP, 2004; Menviel et al., 2020) and yellow bands to Dansgaard Oeschger events (NGRIP, 2004; Menviel et al., 2020)/ Antarctic Isotope Maximum (EPICA, 2006).

6. **Conclusion**

Our new ^{36}Cl CRE age dataset from moraine boulders and glacially polished bedrock surfaces allowed us to refine our understanding of Late Pleistocene glacier fluctuations on Kerguelen. It helped us address the questions of whether glaciers located in the Kerguelen Archipelago *(i)* experienced an early local Last Glacial Maximum during the MIS 3 period in consistency with other regions from the southern mid-latitudes and *(ii)* re-advanced during the gLGM in line with the global-scale maximum extent of mountain glaciers and ice sheets. Moraine mean ages indicate that glacier culminations occurred at ~ 42.2 ka, *i.e.*, during MIS 3, as well as at ~ 21.5 ka and ~ 19.4 ka synchronously with the gLGM. Importantly, this is the first time that MIS 3 and gLGM glacier maxima are demonstrated by moraine dating on the Kerguelen Archipelago. Results from glacially polished bedrock samples span from ~ 39 ka to ~ 19 ka. These ages combined with previously dated bedrock surfaces and erratic boulders suggest that two periods of deglaciation took place on the archipelago during the time interval investigated in this study: the first one right after the ~ 42 ka glacier culmination and the second one after the gLGM. So far there is no evidence of other glacier culminations between these two events. This study also

608 provides evidence of larger glacier extent during MIS 3 than during the gLGM, similar and
609 broadly synchronous with the other southern mid-latitude regions. It appears that Kerguelen
610 multi-millennial glacier evolution may be synchronous with cold temperatures recorded in SST
611 records. However, the reason why glaciers were larger during the MIS 3 than during the gLGM
612 remains puzzling. We hypothesize that precipitation changes may have superimposed on the
613 impact of long-term temperature variations, as Kerguelen is a small archipelago relatively
614 isolated in the southern Indian Ocean, whose glacier change is very sensitive even to minor
615 latitudinal migration of oceanic fronts and the Southern Westerly Winds belt. Changes in these
616 climate mechanisms are also challenging to study other than by local proxies. Therefore, further
617 regional paleoclimatic investigations need to be undertaken to unravel the climatic mechanisms
618 that may have influenced glacier variations in the Kerguelen Archipelago.

619

620 **Author contributions**

621 J.C. designed the paper. V.J., G.D., D.G., V.F., T.R., V.R. and C.L. conducted the fieldwork
622 on the islands. J.C., I.S. and V.J. participated in producing the cosmogenic data. ASTER Team
623 performed accelerator mass spectrometry measurements. J.C., I.S., and V.J. interpreted the
624 cosmogenic ages. J.C. wrote the first draft of the paper and prepared the figures. All authors
625 contributed to the discussion and final version of the manuscript.

626 **Acknowledgments**

627 This work has received financial support from the LabEx DynamiTe (ANR-11-LABX-0046)
628 Les Envahisseurs as part of the 'Investissements d'Avenir' programme. This paper was also
629 supported by the French INSU LEFE Glacepreker project and by the IPEV Kesaaco 1048
630 project. The ^{36}Cl measurements were performed at the ASTER national accelerator mass

spectrometry facility (CEREGE, Aix-en-Provence) that is supported by the INSU/CNRS, the ANR through the 'Projets thématiques d'excellence' programme for the 'Equipements d'excellence' ASTER-CEREGE action and IRD. We are very thankful for the compositional analyses at SARM/CRPG (Nancy, France). We are thankful to the reviewers Elizabeth Rudolph and Attila Çiner, for their positive and constructive comments.

References

Balco, G., Stone, J.O., Lifton, N.A., Dunai, T.J., 2008. A complete and easily accessible means of calculating surface exposure ages or erosion rates from ^{10}Be and ^{26}Al measurements. Quaternary Geochronology, 3 (3), 174-195, https://doi.org/10.1016/j.quageo.2007.12.001.

Berger, A. and Loutre, M.F., 1991. Insolation values for the climate of the last 10 million years. Quaternary Sciences Review, 10 (4), 297-317, 10.1016/0277-3791(91)90033-Q.

Berthier, E., Bris, R. le, Mabileau, L., Testut, L., Rémy, F., 2009. Ice wastage on the Kerguelen Islands (49°S, 69°E) between 1963 and 2006. Journal of Geophysical Research: Earth Surface 114, 1–11. https://doi.org/10.1029/2008JF001192

Borchers, B., Marrero, S., Balco, G., Caffee, M., Goehring, B., Lifton, N., Nishiizumi, K., Phillips, F., Schaefer, J., Stone, J., 2016. Geological calibration of spallation production rates in the CRONUS Earth project. Quat. Geochronol. 31, 188–198. doi:10.1016/j.quageo.2015.01.009

Charton, J., Jomelli, V., Schimmelpfennig, I., Verfaillie, D., Favier, V., Mokadem, F., Gilbert, A., Brun, F., Aumaître, G., Bourlès, D.L., Keddadouche, K., 2020. A debris-covered glacier at Kerguelen (49°S, 69°E) over the past 15 000 years. Antarctic Science, 33(1), 103 - 115, doi: 10.1017/S0954102020000541

Charton, J., Schimmelpfennig, I., Jomelli, V., Delpech, G., Blard, P.-H., Braucher, R., Verfaillie, D., Favier, V., Rinterknecht, V., Goosse, H., Crosta, X., Chassiot, L., Martin, L., Guillaume, D., Legentil, C., ASTER Team, 2022. New cosmogenic nuclide constraints on Late Glacial and Holocene glacier fluctuations in the sub-Antarctic Indian Ocean (Kerguelen Islands, 49°S). Quaternary Science Reviews, 283, 107461, https://doi.org/10.1016/j.quascirev.2022.107461

Çiner, A., Sarıkaya, M.A., Yıldırım, C., Girault, I., Todisco, D., Martin, F., Borrero, L., Fabel, D., 2022. Terrestrial cosmogenic 10Be dating of the Última Esperanza ice lobe moraines (52°S,

662 Patagonia) indicates the global Last Glacial Maximum (LGM) extent was half of the local
663 LGM. Geomorphology, 414, 108381, https://doi.org/10.1016/j.geomorph.2022.108381

664 Civel-Mazens, M., Crosta, X., Cortese, G., Michel, E., Mazaud, A., Ther, O., Ikehara, M., Itaki,
665 T., 2021. Impact of the Agulhas Return Current on the oceanography of the Kerguelen Plateau
666 region, Southern Ocean, over the last 40 kyrs. Quaternary Science Reviews, 251, 106711,
667 10.1016/j.quascirev.2020.106711

668 Clark, P. U., Dyke, A. S., Shakun, J. D., Carlson, A. E., Clark, J., Wohlfarth, B., Mitrovica, J.
669 X., Hostetler, S. W., Marshall McCabe, A., 2009. The last glacial maximum. Science 325, 710-
670 714.

671 Darvill, C.M., Bentley, M.J., Stokes, C.R., Hein, A.S., Rodés, A., 2015. Extensive MIS 3
672 glaciation in southernmost Patagonia revealed by cosmogenic nuclide dating of outwash
673 sediments. Earth and Planetary Science Letters, 429, 157-169,
674 http://dx.doi.org/10.1016/j.epsl.2015.07.030

675 Denton, G.H., Putnam, A.E., Russell, J.L., Barrell, D.J.A., Schaefer, J.M., Kaplan, M.R.,
676 Strand, P.D., 2021. The Zealandia Switch: Ice age climate shifts viewed from Southern
677 Hemisphere moraines. Quaternary Science Reviews, 257, 106771,
678 https://doi.org/10.1016/j.quascirev.2020.106771

679 Doughty, A.M., Schaefer, J.M., Putnam, A.E., Denton, G. H., Kaplan, M.R., Barrell, D.J.A.,
680 Andersen, B.G., Kelley, S.E., Finkel, R.C., Schwartz, R., 2015. Mismatch of glacier extent and
681 summer insolation in Southern Hemisphere mid-latitudes. Geology, 43 (5), 407–410,
682 10.1130/G36477.1.

683 EPICA Community Members, 2006. One-to-one coupling of glacial climate variability in
684 Greenland and Antarctica. Nature, 444, 195–198, 10.1038/nature05301.

685 Favier, V., Verfaillie, D., Berthier, E., Menegoz, M., Jomelli, V., Kay, J.E., Ducret, L.,
686 Malbéteau, Y., Brunstein, D., Gallée, H., Park, Y.H., Rinterknecht, V., 2016. Atmospheric
687 drying as the main driver of dramatic glacier wastage in the southern Indian Ocean. Scientific
688 Reports 6, 1–12. https://doi.org/10.1038/srep3239

689 Fink, D., Vogt, S., Hotchkis, M., 2000. Cross-sections for 36Cl from Ti at Ep ¼ 35-150 MeV:
690 applications to in-situ exposure dating. Nucl. Instrum. Method Phys. Res. B: Beam Interact.
691 Mater. Atoms 172, 861e866. https://doi.org/10.1016/S0168-583X(00)00200-7.

692 García, J.-L., Hein, A. S., Binnie, S. A., Gomez, G. A., Gonzalez, M. A., Dunai, T. J., 2018.
693 The MIS 3 maximum of the Torres del Paine and Última Esperanza ice lobes in Patagonia and
694 the pacing of southern mountain glaciation. Quaternary Science Reviews, 185, 9-26,
695 https://doi.org/10.1016/j.quascirev.2018.01.013

696 Girault, I., Todisco, D., Çiner, A., Sarıkaya, M.A., Yıldırım, C., Quiquerez, A., Martin, F.,
697 Borrero, L., Fabel, D., Grandjean, P., Nehme, C., Mouralis, D., 2022. ^{10}Be chronology of

deglaciation and ice-dammed lake regression in the vicinity of the Mylodon Cave (Cerro Benítez, Patagonia, Chile). Quaternary Science Reviews, 278, 107354, https://doi.org/10.1016/j.quascirev.2021.107354

Giret, A., Weis, D., Grégoire, M., Mattielli, N., Moine, B., Michon, G., Scoates, J., Tourpin, S., Delpech, G., Gerbe, M.-C., Doucet, S., Ethien, R., Cottin, J.-Y., 2003. L'archipel des Kerguelen: les plus vieilles îles dans le plus jeune océan. Géologues, 15–23.

Gillett, N. P., Kell, T. D., Jones, P. D., 2006. Regional climate impacts of the Southern Annular Mode. Geophysical Research Letters, 33, L23704, 10.1029/2006GL027721.

Johnsen, S.J., Dahl-Jensen, D., Gundestrup, N., JSteffensen, J.P., Clausen, H.B., Miller, H., Masson-Delmotte, V., Sveinbjörnsdottir, A.E., White J, 2001. Oxygen isotope and palaeotemperature records from six Greenland ice core stations: Camp Century, Dye 3, GRIP, GISP2, Renland and NorthGRIP. J. Quaternary Sci. 16, 299–307, doi:10.1002/jqs.622.

Jomelli, V., Mokadem, F., Schimmelpfennig, I., Chapron, E., Rinterknecht, V., Favier, V., Verfaillie, D., Brunstein, D., Legentil, C., Michel, E., Swingedouw, D., Jaouen, A., Aumaitre, G., Bourlès, D.L., Keddadouche, K., 2017. Sub-Antarctic glacier extensions in the Kerguelen region (49°S, Indian Ocean) over the past 24,000 years constrained by ^{36}Cl moraine dating. Quaternary Science Reviews 162, 128–144. https://doi.org/10.1016/j.quascirev.2017.03.010

Jomelli, V., Schimmelpfennig, I., Favier, V., Mokadem, F., Landais, A., Rinterknecht, V., Brunstein, D., Verfaillie, D., Legentil, C., Aumaitre, G., Bourlès, D.L., Keddadouche, K., 2018. Glacier extent in sub-Antarctic Kerguelen archipelago from MIS 3 period: Evidence from ^{36}Cl dating. Quaternary Science Reviews 183, 110–123. https://doi.org/10.1016/j.quascirev.2018.01.008

Kaplan, M. R., Coronato, A., Hulton, N. R. J., Rabassa, J. O., Kubik, P. W., Freeman, S.P.H.T., 2007. Cosmogenic nuclide measurements in southernmost South America and implications for landscape change. Geomorphology, 87 (4), 284-301, 10.1016/j.geomorph.2006.10.005

Kelley, S. E., Kaplan, M. R., Schaefer, J. M., Andersen, B. G., Barrell, D. J. A., Putnam, A. E., Denton, G. H., Schwartz, R., Finkel, R. C., Doughty, A. M., 2014. High-precision ^{10}Be chronology of moraines in the Southern Alps indicates synchronous cooling in Antarctica and New Zealand 42,000 years ago. Earth and Planetary Science Letters, 405, 194–206, 10.1016/j.epsl.2014.07.031.

Kiernan, K., Fifield, K.L., Chappell, J., 2004. Cosmogenic nuclide ages for Last Glacial Maximum moraine at Schnells Ridge, Southwest Tasmania. Quaternary Research, 61 (3), 335-338, 10.1016/j.yqres.2004.02.004.

Laj, C., Kissel, C., Beer, J., 2004. High Resolution Global Paleointensity Stack Since 75 kyr (GLOPIS-75) Calibrated to Absolute Values. Timescales Paleomagn. F., Geophysical Monograph Series 145, 255–265. doi:10.1029/145GM19

Leger, T. P. M., Hein, A. S., Bingham, R. G., Rodés, Á., Fabel, D., Smedley, R. K. (2021). Geomorphology and ^{10}Be chronology of the Last Glacial Maximum and deglaciation in northeastern Patagonia, 43°S-71°W. Quaternary Science Reviews, 272, 107194, doi.org/10.1016/j.quascirev.2021.107194.

Marrero, S.M., Phillips, F.M., Caffee, M.W., Gosse, J.C., 2016. CRONUS-Earth cosmogenic ^{36}Cl calibration. Quat. Geochronol. 31, 199-219. https://doi.org/10.1016/j.quageo.2015.10.002.

Matsuoka, K., Skoglund, A., Roth, G., Pomereu, J., Griffiths, H., Headland, R., Herried, B., Katsumata, K., Le Brocq, A., Licht, K., Morgan, F., Neff, P. D., Ritz, C., Scheinert, M., Tamura, T., Van de Putte, A., van den Broeke, M., von Deschwanden, A., Deschamps-Berger, C., Van Liefferinge, B., Tronstad, S., Melvær, Y., 2021. Quantarctica, an integrated mapping environment for Antarctica, the Southern Ocean, and sub-Antarctic islands. Environmental Modelling & Software, 140, 105015, https://doi.org/10.1016/j.envsoft.2021.105015

Mazloff, M. R., Heimbach, P., Wunsch, C., 2010. An Eddy-Permitting Southern Ocean State Estimate. Journal of Physical Oceanography, 40 (5), 880-899, https://doi.org/10.1175/2009JPO4236.1

Menviel, L., Timmermann, A., Elison Timm, O., Mouchet, A., 2011. Deconstructing the Last Glacial termination: the role of millennial and orbital-scale forcings. Quaternary Science Reviews, 30 (9–10), 1155-1172, 10.1016/j.quascirev.2011.02.005.

Menviel, L., Timmerman, A., Friedrich, T., and England, M. H., 2014. Hindcasting the continuum of Dansgaard–Oeschger variability: mechanisms, patterns and timing, Climate of the Past, 10, 63–77, 10.5194/cp-10-63-2014.

Menviel, L.C., Skinner, L.C., Tarasov, L., Tzedakis, P.C., 2020. An ice–climate oscillatory framework for Dansgaard–Oeschger cycles. Nat Rev Earth Environ 1, 677–693, 10.1038/s43017-020-00106-y

Merchel, S., Bremser, W., Alfimov, V., Arnold, M., Aumaître, G., Benedetti, L., Bourles, D.L., Caffee, M., Fifield, L.K., Finkel, R.C., Freeman, S.P.H.T., Martschini, M., Matsushi, Y., Rood, D.H., Sasa, K., Steier, P., Takahashi, T., Tamari, M., Tims, S.G., Tosaki, Y., Wilcken, K.M., Xu, S., 2011. Ultra-trace analysis of 36Cl by accelerator mass spectrometry: an interlaboratory study. Anal. Bioanal. Chem. Res. 400, 3125-3132. https://doi.org/10.1007/s00216-011-4979-2.

North Greenland Ice Core Project members, 2004. High-resolution record of Northern Hemisphere climate extending into the last interglacial period. Nature 431, 147–151, 10.1038/nature02805.

Pahnke, K., Sachs, J.P., 2006. Sea surface temperatures of southern midlatitudes 0-160 kyr BP. Paleoceanography 21, PA2004. https://doi.org/10.1029/2005PA001191.

769 Ponthus, L., 2018. Origine, evolution et mise en place d'un pluton recent en contexte
770 intraplaque oceanique. Exemple du complexe sud de Rallier du Baty, Kerguelen (T.A.A.F.).
771 Ph.D. thesis. Universite Toulouse 3 Paul Sabatier, France.

772 Putnam, A. E., Schaefer, J. M., Denton, G. H., Barrell, Birkel, S. D., D. J. A., Andersen, B. G.,
773 Kaplan, M. R., Finkel, R. C., Schwartz, R., Doughty, A. M, 2013. The Last Glacial Maximum
774 at 44°S documented by a 10Be moraine chronology at Lake Ohau, Southern Alps of New
775 Zealand. Quaternary Science Reviews, 62, 114-141, 10.1016/j.quascirev.2012.10.034

776 Rasmussen, S.O., Bigler, M., Blockley, S.P., Blunier, T., Buchardt, S.L., Clausen, H.B.,
777 Cvijanovic, I., Dahl-Jensen, D., Johnsen, S.J., Fischer, H., Gkinis, V., Guillevic, M., Hoek,
778 W.Z., Lowe, J.J., Pedro, J.B., Popp, T., Seierstad, I.K., Steffensen, J.P., Svensson, A.M.,
779 Vallelonga, P., Vinther, B.M., Walker, M.J.C., Wheatley, J.J., Winstrup, M., 2014. A
780 stratigraphic framework for abrupt climatic changes during the Last Glacial period based on
781 three synchronized Greenland ice-core records: refining and extending the INTIMATE event
782 stratigraphy, Quaternary Science Reviews, 106, 14-28,
783 https://doi.org/10.1016/j.quascirev.2014.09.007

784 Raup, B., Racoviteanu, A., Khalsa, S.J.S., Helm, C., Armstrong, R., Arnaud, Y., 2007. The
785 GLIMS geospatial glacier database: a new tool for studying glacier change. Global Planetary
786 Change, 56, https://doi.org/10.1016/j.gloplacha.2006.07.018.

787 Rudolph, E.M., Hedding, D.W., Fabel, D., Hodgson, D.A., Gheorghiu, D.M., Shanks, R., Nel,
788 W, 2020. Early glacial maximum and deglaciation at sub-Antarctic Marion Island from
789 cosmogenic ^{36}Cl exposure dating. Quaternary Science Reviews, 231,
790 10.1016/j.quascirev.2020.106208

791 Sallée, J. B., Speer, K., Morrow, R., 2008. Response of the Antarctic Circumpolar Current to
792 Atmospheric Variability. J. Clim. 21, 3020–3039, 10.1175/2007JCLI1702.1.

793 Schimmelpfennig, I., 2009. Cosmogenic ^{36}Cl in Ca and K rich minerals: analytical
794 developments, production rate calibrations and cross calibration with ^{3}He and ^{21}Ne, Ph.D.
795 thesis, Université Paul Cézanne - Aix-Marseille III, France.

796 Schimmelpfennig, I., Benedetti, L., Finkel, R., Pik, R., Blard, P.H., Bourlès, D., Burnard, P.,
797 Williams, A., 2009. Sources of in-situ ^{36}Cl in basaltic rocks. Implications for calibration of
798 production rates. Quaternary Geochronology 4, 441–461.
799 https://doi.org/10.1016/j.quageo.2009.06.003

800 Schimmelpfennig, I., Benedetti, L., Garreta, V., Pik, R., Blard, P.H., Burnard, P., Bourlès, D.,
801 Finkel, R., Ammon, K., Dunai, T., 2011. Calibration of cosmogenic ^{36}Cl production rates from
802 Ca and K spallation in lava flows from Mt. Etna (38°N, Italy) and Payun Matru (36°S,
803 Argentina). Geochimica et Cosmochimica Acta 75, 2611–2632.
804 https://doi.org/10.1016/j.gca.2011.02.013

Schimmelpfennig, I., Schaefer, J.M., Putnam, A.E., Koffman, T., Benedetti, L., Ivy-Ochs, S., Schlüchter, C., Arnold, M., Aumaître, G., Bourlès, D., Keddadouche, K., 2014. ^{36}Cl production rate from K-spallation in the European Alps (Chironico landslide, Switzerland). Journal of Quaternary Science 29, 407–413. https://doi.org/10.1002/jqs.2720

Sokolov, S., Rintoul, S.R., 2009. Circumpolar structure and distribution of the Ant- arctic Circumpolar Current fronts: 2. Variability and relationship to sea surface height. J. Geophys. Res. 114 https://doi.org/10.1029/2008JC005248

Stone, J.O., 2000. Isotope production. Journal of Geophysical Research, 105, 753–759.

Stone, J.O., Fifield, K., Vasconcelos, P., 2005. Terrestrial chlorine-36 production from spallation of iron, in: Abstract of 10th International Conference on Accelerator Mass Spectrometry.

Strand, P. D., Schaefer, J. M., Putnam, A. E., Denton, G. H., Barrell, D. J. A., Koffman, T. N. B., Roseanne Schwartz, R., 2019. Millennial-scale pulsebeat of glaciation in the Southern Alps of New Zealand. Quaternary Science Reviews, 220, 165-177, https://doi.org/10.1016/j.quascirev.2019.07.022

Tielidze, L. G., Eaves, S. R., Norton, K. P., Mackintosh, A. N., Hidy, A. J., 2022. Cosmogenic ^{10}Be constraints on deglacial snowline rise in the Southern Alps, New Zealand. Quaternary Science Reviews, 286, 107548, https://doi.org/10.1016/j.quascirev.2022.107548

Uppala, S.M., Kållberg, P.W., Simmons, A.J., Andrae, U., Bechtold, V.D.C., Fiorino, M., Gibson, J.K., Haseler, J., Hernandez, A., Kelly, G.A., Li, X., Onogi, K., Saarinen, S., Sokka, N., Allan, R.P., Andersson, E., Arpe, K., Balmaseda, M.A., Beljaars, A.C.M., Berg, L.V.D., Bidlot, J., Bormann, N., Caires, S., Chevallier, F., Dethof, A., Dragosavac, M., Fisher, M., Fuentes, M., Hagemann, S., Holm, E., Hoskins, B.J., Isaksen, L., Janssen, P.A.E.M., Jenne, R., Mcnally, A.P., Mahfouf, J.-F., Morcrette, J.-J., Rayner, N.A., Saunders, R.W., Simon, P., Sterl, A., Trenberth, K.E., Untch, A., Vasiljevic, D., Viterbo, P., Woollen, J., 2005. The ERA-40 re-analysis. Q. J. R. Meteorol. Soc. 131, 2961e3012. https://doi.org/10.1256/qj.04.176.

Verfaillie, D., Favier, V., Dumont, M., Jomelli, V., Gilbert, A., Brunstein, D., Gallée, H., Rinterknecht, V., Menegoz, M., Frenot, Y., 2015. Recent glacier decline in the Kerguelen Islands (49°S, 69°E) derived from modeling , field observations , and satellite data. Journal of Geophysical Research: Earth Surface 120, 637–654. https://doi.org/10.1002/2014JF003329.

Verfaillie, D., Charton, J., Schimmelpfennig, I., Stroebele, Z., Jomelli, V., Bétard, F., Favier, V., Cavero, J., Berthier, E., Goosse, H., Rinterknecht, V., Legentil, C., Charrassin, R., Aumaître, G., Bourlès, D.L., Keddadouche, K., 2021. Evolution of the Cook Ice Cap (Kerguelen Islands) between the last centuries and 2100 CE based on cosmogenic dating and glacio-climatic modelling. Antarctic Science, 33(3), 301-317. doi:10.1017/S0954102021000080

WAIS Divide Project Members, 2015. Precise interpolar phasing of abrupt climate change during the last ice age. Nature, 520, 661–665, 10.1038/nature14401.

Ward, G.K., Wilson, S.R., 1978. Procedures for comparing and combining radiocarbon age determinations: A critique. Archaeometry 20, 19–31, doi: 10.1111/j.1475-4754.1978.tb00208.x.

Whittaker, T. E., Hendy, C. H., Hellstrom, J. C., 2011. Abrupt millennial-scale changes in intensity of Southern Hemisphere westerly winds during marine isotope stages 2–4, Geology, 39 (5), 455–458, 10.1130/G31827.1.

Zech, R., Kull, Ch., Kubik, P. W., Veit, H., 2007. Exposure dating of Late Glacial and pre-LGM moraines in the Cordon de Dona Rosa, Northern/Central Chile (∼31°S). Climate of the Past, 3, 1–14, 10.5194/cp-3-1-2007.

Zech, R., Zech, J., Kull, Ch., Kubik, P. W., Veit, H., 2011. Early last glacial maximum in the southern Central Andes reveals northward shift of the westerlies at ~39 ka. Climate of the Past, 7 (1), 41–46, 10.5194/cp-7-41-2011

Table 1: Geographic sample locations. topographic shielding factors. sample thicknesses. and formation age of rock.

Sample Name	Latitude (°S)	Longitude (°E)	Elevation (m)	Shielding factor	Thickness (cm)
Port-aux-Français site					
Till (inboard PAF moraine)					
PAF-03	49.30766	70.33690	58	0.998	3
PAF moraine					
PAF-01	49.32636	70.30222	41	0.999	3
PAF-02	49.30022	70.36621	71	0.999	4
PAF-04	49.35143	70.29258	32	0.999	2
PAF-05	49.35149	70.29245	27	0.998	5
PAF-06	49.35366	70.28725	36	0.999	2
Port Jeanne D'Arc site					
PJDA moraine					
PJDA-02	49.54310	69.78761	33	0.998	2
PJDA-04	49.54381	69.79069	27	0.994	3
Glacially polished bedrocks					
PJDA-05	49.59253	69.82333	260	0.998	2
PJDA-10	49.59112	69.82365	480	0.998	2
PJDA-11	49.59112	69.82365	480	0.994	3
PJDA-13	49.59112	69.82365	480	0.994	3
Baie Larose site					
B1 moraine					
BLR-01	49.55507	69.36555	81	0.998	3
BLR-02	49.55509	69.36559	79	0.998	5
BLR-03	49.55685	69.36816	79	0.998	3
BLR-04	49.55752	69.36758	79	0.998	3
BLR-05	49.55782	69.36781	83	0.998	3
B2 moraine					
BLR-06	49.55428	69.37249	113	0.999	3
BLR-07	49.55605	69.37518	116	0.999	3
Longue Island site					
glacially polished bedrocks					
LON-01	49.51610	69.87526	110	0.988	3
LON-02	49.51610	69.87526	110	0.988	5
LON-03	49.51610	69.87526	110	0.988	3
Australia Island site					
glacially polished bedrocks					
AUS-02	49.42806	69.82468	62	0.985	2
AUS-05	49.42805	69.82467	62	0.985	3
McMurdo Island site					
glacially polished bedrocks					
MCM-02	48.89502	69.41628	151	0.997	4
MCM-05	48.89502	69.41628	151	0.997	2

Table 2: Chemical compositions of the bulk rock samples before chemical treatment. Analysis performed at the SARM-CRPG (Nancy, France) by ICP-OES (major elements), ICP-MS (trace element), atomic absorption (Li), colorimetry (B) and spectrophotometry (Cl).

Sample Name	CaO %	K_2O %	TiO_2 %	Fe_2O_3 %	Cl (ppm)	SiO_2 %	Na_2O %	MgO %	Al_2O_3 %	MnO %	P_2O_5 %	CO_2 %	Li (ppm)	B (ppm)	Sm (ppm)	Gd (ppm)	Th (ppm)	U (ppm)	LOI
Port-aux-Français site																			
Till (inboard PAF moraine)																			
PAF-03	8.02	1.14	2.39	12.41	92	45.58	2.91	8.51	14.10	0.17	0.52	0.80	8.08	3.70	6.46	5.40	5.05	1.04	3.43
PAF moraine																			
PAF-01	8.22	0.67	1.74	13.53	92	44.44	1.87	15.02	11.13	0.17	0.23	1.98	5.54	2.40	3.42	3.26	1.40	0.31	3.29
PAF-02	7.84	0.54	1.62	13.13	67	45.09	2.14	10.53	12.79	0.17	0.19	1.61	4.21	<2	3.52	3.59	1.42	0.30	5.42
PAF-04	10.38	1.39	3.14	11.31	33	44.72	2.64	3.97	18.61	0.14	0.40	1.80	6.47	<2	6.30	5.65	3.36	0.73	2.62
PAF-05	8.62	0.93	2.22	12.59	64	44.96	2.39	9.51	14.16	0.16	0.34	1.80	6.08	2.53	4.92	4.47	2.81	0.60	3.69
PAF-06	8.62	0.93	2.22	12.59	64	44.96	2.39	9.51	14.16	0.16	0.34	1.80	6.08	2.53	4.92	4.47	2.81	0.60	3.69
Port Jeanne D'Arc site																			
PJDA moraine																			
PJDA-02	11.20	0.80	1.85	9.68	35	47.41	3.16	2.82	20.83	0.12	0.25	-	5.37	<2	3.93	3.70	1.80	0.40	1.11
PJDA-04	11.00	1.11	1.28	7.70	50	47.38	3.14	2.26	22.68	0.10	0.33	1.21	6.86	2.40	3.74	3.25	2.35	0.48	3.51
Glacially polished bedrocks																			
PJDA-05	4.30	3.68	1.55	11.59	76	51.05	4.55	2.34	17.16	0.17	1.39	0.64	14.90	2.90	10.30	7.64	10.07	2.08	2.11
PJDA-10	7.40	1.12	3.16	13.33	61	44.05	3.30	8.60	13.31	0.17	0.64	-	9.20	3.40	8.56	7.23	5.91	1.29	3.61
PJDA-11	7.67	0.95	3.15	13.18	69	44.50	3.47	8.42	13.38	0.17	0.64	-	10.49	3.77	8.57	7.18	5.84	1.21	3.95
PJDA-13	7.94	0.77	3.14	13.03	70	44.95	3.64	8.25	13.45	0.18	0.63	0.75	7.38	5.00	8.57	7.14	5.77	1.14	4.29
Baie Larose site																			
B1 moraine																			
BLR-01	11.39	0.77	1.43	7.79	<20	45.93	2.68	3.04	21.49	0.10	0.19	-	5.01	<2	3.19	2.94	1.28	0.28	4.43
BLR-02	11.24	0.77	1.71	9.19	26	46.40	2.90	3.01	20.73	0.12	0.23	-	5.33	<2	3.58	3.34	1.54	0.34	3.11
BLR-03	10.15	0.93	2.33	12.05	<20	46.44	3.16	3.37	17.96	0.16	0.31	-	6.75	<2	4.67	4.45	2.10	0.46	2.80
BLR-04	11.24	0.77	1.71	9.19	26	46.40	2.90	3.01	20.73	0.12	0.23	-	5.33	<2	3.58	3.34	1.54	0.34	3.11
BLR-05	12.19	0.61	1.38	7.73	37	46.84	2.85	2.61	22.73	0.09	0.19	-	4.24	<2	2.88	2.64	1.23	0.27	2.09
B2 moraine																			
BLR-06	11.49	0.67	1.38	8.28	25	46.70	2.80	3.36	21.77	0.10	0.20	-	4.95	<2	3.21	3.03	1.42	0.30	2.48
BLR-07	11.49	0.67	1.38	8.28	25	46.70	2.80	3.36	21.77	0.10	0.20	-	4.95	<2	3.21	3.03	1.42	0.30	2.48
Longue Island site																			
glacially polished bedrocks																			
LON-01	8.26	1.62	3.01	12.21	46	47.63	3.34	3.82	16.70	0.16	0.50	-	7.43	<2	7.09	6.43	3.75	0.82	2.21
LON-02	8.26	1.62	3.01	12.21	46	47.63	3.34	3.82	16.70	0.16	0.50	-	7.43	<2	7.09	6.43	3.75	0.82	2.21
LON-03	8.26	1.62	3.01	12.21	46	47.63	3.34	3.82	16.70	0.16	0.50	-	7.43	<2	7.09	6.43	3.75	0.82	2.21
Australia Island site																			
glacially polished bedrocks																			
AUS-02	6.81	1.71	3.43	15.27	125	45.87	3.51	4.85	15.86	0.19	0.55	0.79	11.0	4.80	7.44	6.50	4.86	1.05	1.77
AUS-05	6.75	1.74	3.50	15.12	130	46.49	3.56	4.71	16.11	0.19	0.53	0.68	11.2	5.40	7.47	6.62	4.85	1.07	1.58
McMurdo Island site																			
glacially polished bedrocks																			
MCM-02	9.78	0.46	1.46	11.75	57	45.09	2.33	8.50	15.78	0.17	0.18	0.22	5.44	2.50	3.30	3.33	0.61	0.14	4.90
MCM-05	9.78	0.46	1.46	11.75	57	45.09	2.33	8.50	15.78	0.17	0.18	0.22	5.44	2.50	3.30	3.33	0.61	0.14	4.90

Table 3: Concentrations of the major element oxides, determined in splits taken from the samples after the chemical pre-treatment (acid etching). Analysis performed at the SARM-CRPG (Nancy, France) by ICP-OES.

Sample Name	CaO %	K_2O %	TiO_2 %	Fe_2O_3 %	SiO_2 %	Na_2O %	MgO %	Al_2O_3 %	MnO %	P_2O_5 %	LOI
Port-aux-Français site											
Till (inboard PAF moraine)											
PAF-03	8.73 ± 0.44	1.39 ± 0.14	2.96 ± 0.30	10.66 ± 0.21	51.15	3.14	6.31	13.53	0.13	0.18	0.65
PAF moraine											
PAF-01	9.86 ± 0.49	0.79 ± 0.16	2.44 ± 0.24	11.13 ± 0.22	48.79	2.22	10.33	11.36	0.14	0.10	1.63
PAF-02	9.40 ± 0.47	0.62 ± 0.12	2.26 ± 0.23	9.87 ± 0.99	53.17	2.49	7.53	11.46	0.14	< L.D. (0.10)	1.93
PAF-04	10.27 ± 0.21	1.36 ± 0.14	4.65 ± 0.47	13.10 ± 0.26	48.11	2.50	3.84	14.64	0.15	0.10	0.51
PAF-05	8.19 ± 0.41	1.12 ± 0.11	3.60 ± 0.36	14.18 ± 0.28	46.61	2.53	9.96	12.36	0.15	< L.D. (0.10)	0.22
PAF-06	8.79 ± 0.44	1.27 ± 0.13	3.27 ± 0.33	12.84 ± 0.26	49.89	3.00	5.10	14.64	0.16	< L.D. (0.10)	-0.29
Port Jeanne D'Arc site											
PJDA moraine											
PJDA-02	11.15 ± 0.22	0.83 ± 0.17	2.06 ± 0.21	8.04 ± 0.80	51.11	3.26	2.44	19.82	0.11	< L.D. (0.10)	-0.17
PJDA-04	12.26 ± 0.25	0.60 ± 0.12	1.52 ± 0.15	5.38 ± 0.54	51.50	2.85	1.77	22.13	0.08	< L.D. (0.10)	1.25
Glacially polished bedrocks											
PJDA-05	3.39 ± 0.51	4.27 ± 0.43	1.74 ± 0.17	7.86 ± 0.79	56.93	5.20	0.45	18.35	0.08	0.52	0.32
PJDA-10	8.31 ± 0.42	1.16 ± 0.12	3.97 ± 0.40	10.66 ± 0.21	51.62	3.45	4.98	13.15	0.12	0.34	1.43
PJDA-11	8.28 ± 0.41	1.15 ± 0.12	3.95 ± 0.40	11.03 ± 0.22	50.69	3.70	5.13	13.15	0.13	0.43	2.06
PJDA-13	8.17 ± 0.41	0.89 ± 0.18	3.75 ± 0.38	11.03 ± 0.22	50.69	3.70	5.13	13.15	0.13	0.43	2.06
Baie Larose site											
B1 moraine											
BLR-01	14.20 ± 0.28	0.14 ± 0.04	0.08 ± 0.02	0.74 ± 0.11	51.61	2.55	0.17	29.15	< L.D. (0.015)	< L.D. (0.10)	0.57
BLR-02	14.33 ± 0.29	0.15 ± 0.04	0.09 ± 0.02	0.88 ± 0.18	50.60	2.51	0.22	29.25	< L.D. (0.015)	< L.D. (0.10)	1.53
BLR-03	9.94 ± 0.50	1.11 ± 0.11	2.59 ± 0.26	8.29 ± 0.83	53.70	3.41	2.94	16.34	0.14	0.10	1.56
BLR-04	11.82 ± 0.24	0.65 ± 0.13	0.13 ± 0.03	0.90 ± 0.14	44.02	2.17	0.41	24.97	< L.D. (0.015)	< L.D. (0.10)	14.19
BLR-05	14.66 ± 0.29	0.14 ± 0.03	0.10 ± 0.02	0.95 ± 0.14	50.04	2.59	0.23	29.96	< L.D. (0.015)	< L.D. (0.10)	0.90
B2 moraine											
BLR-06	14.54 ± 0.29	0.20 ± 0.05	0.13 ± 0.03	0.98 ± 0.15	50.35	2.60	0.42	29.36	< L.D. (0.015)	< L.D. (0.10)	1.16
BLR-07	15.40 ± 0.31	0.10 ± 0.02	0.07 ± 0.02	0.67 ± 0.10	49.49	1.98	0.19	30.48	< L.D. (0.015)	< L.D. (0.10)	1.07
Longue Island site											
glacially polished bedrocks											
LON-01	8.48 ± 0.42	1.70 ± 0.17	4.04 ± 0.40	10.60 ± 0.21	51.27	3.54	2.85	16.50	0.14	< L.D. (0.10)	0.80
LON-02	8.47 ± 0.42	1.76 ± 0.18	3.97 ± 0.40	10.64 ± 0.21	51.64	3.49	2.89	16.45	0.13	< L.D. (0.10)	-0.30
LON-03	7.66 ± 0.38	1.75 ± 0.17	4.20 ± 0.42	12.42 ± 0.25	50.42	3.48	2.53	15.82	0.11	< L.D. (0.10)	0.50
Australia Island site											
glacially polished bedrocks											
AUS-02	7.07 ± 0.35	1.92 ± 0.19	4.04 ± 0.40	12.63 ± 0.25	49.64	3.95	2.54	16.57	0.15	0.19	0.32
AUS-05	6.93 ± 0.35	1.87 ± 0.19	4.21 ± 0.42	13.34 ± 0.27	49.81	3.89	2.52	16.26	0.16	0.20	0.28
McMurdo Island site											
glacially polished bedrocks											
MCM-02	9.25 ± 0.46	0.40 ± 0.10	2.52 ± 0.25	15.61 ± 0.31	50.82	2.26	5.64	11.41	0.17	0.10	2.43
MCM-05	11.28 ± 0.23	0.38 ± 0.10	2.48 ± 0.25	9.54 ± 0.95	51.92	2.39	5.98	13.08	0.17	0.16	2.13

Table 4: ^{36}Cl dating results. Spike is enriched in ^{35}Cl (~99.66%). ^{36}Cl/^{35}Cl and ^{35}Cl/^{37}Cl ratios were inferred from measurements at the AMS facility ASTER after normalization to the inhouse standard SM-CL-12, using an assigned value of 1.428 (± 0.021) x 10^{-12} for the ^{36}Cl/^{35}Cl ratio (Merchel et al., 2011) and assuming a natural ratio of 3.127 for the stable ratio ^{35}Cl/^{37}Cl. Samples in italic were rejected as outliers and excluded from mean age calculations.

Sample Name	Sample weight (g)	mass of Cl in spike (mg)	^{35}Cl/^{37}Cl	^{36}Cl/^{35}Cl (10^{-14})	[Cl] in sample (ppm)	[^{36}Cl] (10^3 atoms g^{-1})	Age (yr)[a]	Arithmetic mean age (yr)	Chi^2 test
Port-aux-Français site									
Erratic boulder (in till inboard of PAF moraine)									
PAF-03	38.55	1.813	20.91 ± 0.52	20.59 ± 1.04	10.0	193.1 ± 10.3	34700 ± 4000 (3300)	-	-
PAF moraine									
PAF-01	43.39	1.819	19.42 ± 0.49	25.81 ± 1.32	9.8	218.7 ± 11.8	43500 ± 5500 (4300)	42200 ± 4900	Accepted
PAF-02	38.17	1.811	22.33 ± 0.39	23.29 ± 1.20	9.3	217.9 ± 11.8	46100 ± 5800 (4500)		Accepted
PAF-04	*39.33*	*2.026*	*26.66 ± 0.65*	*47.04 ± 2.44*	*3.6*	*465.7 ± 24.3*	*84300 ± 10200 (8100)*		*Rejected*
PAF-05	*46.05*	*2.021*	*19.31 ± 0.35*	*58.11 ± 3.01*	*6.6*	*516.4 ± 26.9*	*116600 ± 14800 (12000)*		*Rejected*
PAF-06	46.23	2.022	12.35 ± 0.20	22.86 ± 1.25	15.0	227.1 ± 12.5	41200 ± 4800 (3900)		Accepted
Port Jeanne D'Arc site									
PJDA moraine									
PJDA-02	46.64	2.033	16.45 ± 0.28	12.79 ± 0.78	12.6	116.0 ± 7.2	20400 ± 2500 (2000)	21500 ± 3200	Accepted
PJDA-04	44.14	1.815	52.52 ± 0.91	16.19 ± 1.08	2.6	119.9 ± 8.0	22700 ± 3000 (2200)		Accepted
Glacially polished bedrocks									
PJDA-05	37.50	1.814	10.59 ± 0.24	27.28 ± 1.38	25.8	317.6 ± 19.3	33400 ± 4200 (3800)	-	-
PJDA-10	40.54	2.034	15.29 ± 0.27	35.62 ± 1.84	16.0	380.5 ± 19.9	49200 ± 5400 (4200)	-	Rejected
PJDA-11	37.91	2.090	16.83 ± 0.30	25.81 ± 1.31	15.5	295.8 ± 15.2	38000 ± 4100 (3200)	-	Rejected
PJDA-13	41.25	1.812	18.23 ± 0.41	20.98 ± 1.50	11.1	188.6 ± 14.0	26500 ± 3400 (2800)	-	Rejected
Baie Larose site									
B1 moraine									
BLR-01	28.40	2.013	95.13 ± 2.93	8.48 ± 0.54	0	103.8 ± 6.7	19500 ± 2700 (1700)	21400 ± 3700	Accepted
BLR-02	29.57	2.049	82.16 ± 3.70	11.46 ± 2.55	2.2	138.8 ± 31.2	25100 ± 6500 (6000)		Accepted
BLR-03	60.91	1.999	16.64 ± 1.05	16.01 ± 0.91	7.1	109.1 ± 6.5	19100 ± 2200 (1800)		Accepted
BLR-04	26.77	2.036	104.70 ± 1.72	9.90 ± 0.59	1.5	130.3 ± 7.9	24800 ± 3200 (2300)		Accepted
BLR-05	25.39	2.039	120.97 ± 2.04	7.53 ± 0.58	1.1	103.8 ± 8.2	18300 ± 2600 (1800)		Accepted
B2 moraine									
BLR-06	29.93	2.034	75.06 ± 1.37	9.71 ± 0.65	2.5	115.5 ± 7.9	19500 ± 2600 (1800)	19400 ± 2600	Accepted
BLR-07	33.74	2.030	103.62 ± 1.84	11.18 ± 0.72	1.2	116.6 ± 7.6	19200 ± 2600 (1700)		Accepted
Longue Island site									
glacially polished bedrocks									
LON-01	39.92	1.985	12.19 ± 0.39	22.57 ± 1.26	17.3	255.9 ± 14.7	39600 ± 4600 (3800)	39500 ± 4600	Accepted
LON-02	42.56	2.043	13.75 ± 0.24	42.09 ± 1.34	13.7	253.9 ± 14.3	39600 ± 4500 (3900)		Accepted
LON-03	37.77	2.032	6.93 ± 0.24	17.74 ± 0.94	52.8	295.1 ± 17.8	39200 ± 4800 (3700)		Accepted
Australia Island site									
glacially polished bedrocks									
AUS-02	40.78	1.818	8.51 ± 0.16	11.65 ± 0.75	33.3	139.1 ± 10.8	20800 ± 2600 (2300)	22100 ± 3500	Accepted
AUS-05	40.73	1.818	6.65 ± 0.21	11.78 ± 0.76	51.4	168.3 ± 14.8	23400 ± 3200 (2800)		Accepted
McMurdo Island site									
glacially polished bedrocks									
MCM-02	41.47	1.993	13.66 ± 0.41	10.44 ± 0.62	13.7	110.1 ± 6.6	21500 ± 2700 (2000)	19200 ± 4000	Accepted
MCM-05	24.63	1.811	68.62 ± 1.33	7.07 ± 0.49	3.2	92.0 ± 6.4	17000 ± 2200 (1600)		Accepted

Blanks[b]					Total atoms Cl (10^{17})	Total atoms ^{36}Cl (10^4)			
Bk6	-	1.801	213.3 ± 6.8	0.036 ± 0.025	1.71 ± 0.27	1.11 ± 0.79	-	-	-
Bk9	-	2.016	50.0 ± 1.7	0.130 ± 0.032	25.31 ± 1.19	4.73 ± 1.16	-	-	-
Bk10	-	1.938	41.1 ± 0.8	0.042 ± 0.020	31.11 ± 0.92	1.51 ± 0.70	-	-	-
Bk11	-	2.029	200.3 ± 5.9	0.113 ± 0.036	2.37 ± 0.22	4.0 ± 1.3	-	-	-

[a] Age uncertainties are reported at 1 sigma level and were calculated through full propagation of analytical and production rate errors. Numbers in brackets are analytical uncertainties only.

[b] Bk6 was processed with the samples PAF-01, -02, -03, PJDA-04, -05, -13, AUS-02, -05 and MCM-05. Bk9 was processed with BLR-01, -03. Bk10 was processed with MCM-02, PAF-04, -05, -06, LON-01, -02, -03. Bk11 was processed with PJDA-02, -10, -11, BLR-02, -04, -05, -06 and -07.